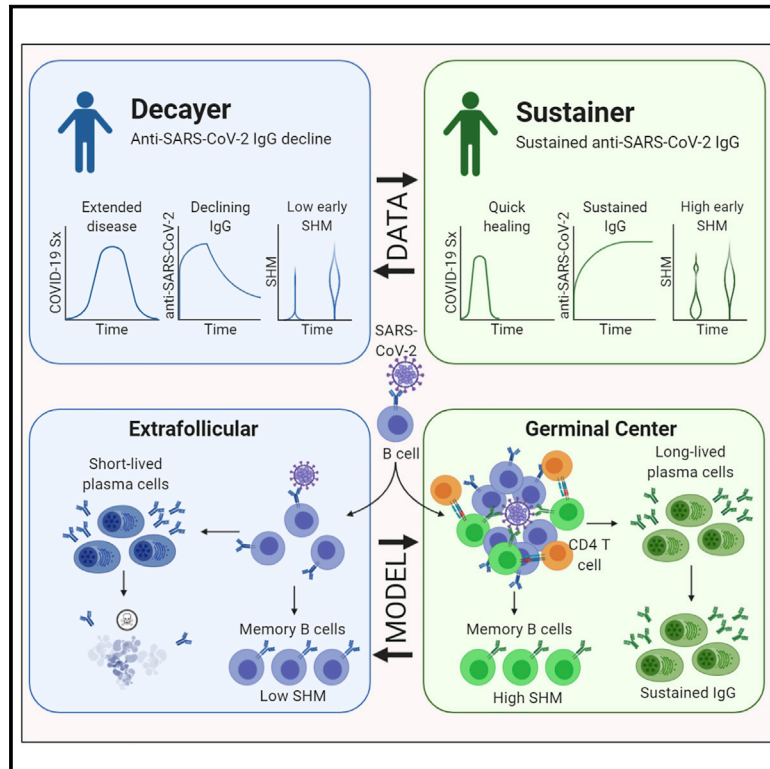


# Quick COVID-19 Healers Sustain Anti-SARS-CoV-2 Antibody Production

## Graphical Abstract



## Authors

Yuezhou Chen, Adam Zuiani,  
Stephanie Fischinger, ...,  
Douglas A. Lauffenburger, Galit Alter,  
Duane R. Wesemann

## Correspondence

dwesemann@bwh.harvard.edu

## In Brief

Longitudinal analyses of antibody responses to SARS-CoV-2 demonstrate that individuals with sustained virus-specific IgG production have shorter disease trajectories, with a subset demonstrating increased somatic hypermutation and higher levels of activated CD4<sup>+</sup> cells.

## Highlights

- SARS-CoV-2 antibody responses range from negligible to robust in mild COVID-19
- Some individuals maintain stable or increased SARS-CoV-2 IgG, while most decline
- Those who sustain virus-specific IgG production tend to have shorter disease courses
- Virus-specific B cells from “sustainers” have more SHM early after disease resolution



## Article

# Quick COVID-19 Healers Sustain Anti-SARS-CoV-2 Antibody Production

Yuezhou Chen,<sup>1,8</sup> Adam Zuiani,<sup>1,8</sup> Stephanie Fischinger,<sup>2</sup> Jyotsna Mullur,<sup>1</sup> Caroline Atyeo,<sup>2</sup> Meghan Travers,<sup>1</sup> Felipe J.N. Leles,<sup>1</sup> Krista M. Pullen,<sup>3</sup> Hannah Martin,<sup>1</sup> Pei Tong,<sup>1</sup> Avneesh Gautam,<sup>1</sup> Shaghayegh Habibi,<sup>1</sup> Jillian Bensko,<sup>1</sup> Deborah Gakpo,<sup>1</sup> Jared Feldman,<sup>2</sup> Blake M. Hauser,<sup>2</sup> Timothy M. Caradonna,<sup>2</sup> Yongfei Cai,<sup>4</sup> John S. Burke,<sup>2</sup> Junrui Lin,<sup>1</sup> James A. Lederer,<sup>5,7</sup> Evan Christopher Lam,<sup>2</sup> Christy L. Lavine,<sup>6</sup> Michael S. Seaman,<sup>6</sup> Bing Chen,<sup>4,6</sup> Aaron G. Schmidt,<sup>2,7</sup> Alejandro Benjamin Balazs,<sup>2,7</sup> Douglas A. Lauffenburger,<sup>3,7</sup> Galit Alter,<sup>2,7</sup> and Duane R. Wesemann<sup>1,7,9,\*</sup>

<sup>1</sup>Department of Medicine, Division of Allergy and Immunology, Division of Genetics, Brigham and Women's Hospital, Harvard Medical School, Boston, MA 02115, USA

<sup>2</sup>Ragon Institute of MGH, MIT, and Harvard, Cambridge, MA 02139, USA

<sup>3</sup>Massachusetts Institute of Technology, Cambridge, MA 02139, USA

<sup>4</sup>Boston Children's Hospital, Boston, MA 02115, USA

<sup>5</sup>Department of Surgery, Brigham and Women's Hospital and Harvard Medical School, Boston, MA 02115, USA

<sup>6</sup>Center for Virology and Vaccine Research, Beth Israel Deaconess Medical Center, Boston, MA, USA

<sup>7</sup>Massachusetts Consortium on Pathogen Readiness, Boston, MA 02115, USA

<sup>8</sup>These authors contributed equally

<sup>9</sup>Lead Contact

\*Correspondence: [dwesemann@bwh.harvard.edu](mailto:dwesemann@bwh.harvard.edu)

<https://doi.org/10.1016/j.cell.2020.10.051>

## SUMMARY

Antibodies are key immune effectors that confer protection against pathogenic threats. The nature and longevity of the antibody response to SARS-CoV-2 infection are not well defined. We charted longitudinal antibody responses to SARS-CoV-2 in 92 subjects after symptomatic COVID-19. Antibody responses to SARS-CoV-2 are unimodally distributed over a broad range, with symptom severity correlating directly with virus-specific antibody magnitude. Seventy-six subjects followed longitudinally to ~100 days demonstrated marked heterogeneity in antibody duration dynamics. Virus-specific IgG decayed substantially in most individuals, whereas a distinct subset had stable or increasing antibody levels in the same time frame despite similar initial antibody magnitudes. These individuals with increasing responses recovered rapidly from symptomatic COVID-19 disease, harbored increased somatic mutations in virus-specific memory B cell antibody genes, and had persistent higher frequencies of previously activated CD4<sup>+</sup> T cells. These findings illuminate an efficient immune phenotype that connects symptom clearance speed to differential antibody durability dynamics.

## INTRODUCTION

Coronavirus disease 2019 (COVID-19), caused by severe acute respiratory syndrome coronavirus 2 (SARS-CoV-2), is a major global threat. COVID-19 shows remarkable heterogeneity spanning from asymptomatic to lethal infections (Wu and McGoogan, 2020; Zhou et al., 2020; Zhu et al., 2020). There is a critical need to understand the nature of the immune response to SARS-CoV-2 to shed light on requirements and likelihood for durable protective immunity in humans.

Antibodies are secreted effector molecules produced as dimers of immunoglobulin (Ig) heavy (H) and light (L) chain pairs from B lineage cells and come in various IgH isotypes (e.g., IgM, IgG, IgA). Antibody responses to initial infection can reduce the probability of getting sick from the same pathogen more than once. Upon a first-time infection, the antibody system can learn

to better recognize the pathogen through a process of B cell clonal selection and somatic hypermutation (SHM) and then produce these improved versions of antibodies in greater amounts to prophylax for a future encounter by the pathogen.

After primary infection or vaccination, IgG antibody production can be maintained and protect for decades as is the case for diphtheria, varicella-zoster, and measles (Amanna et al., 2007). Durable antibody responses like these rely on coordinated T and B lymphocyte interactions within lymphoid tissue germinal centers (GCs). Activated B cells within GCs diversify Ig genes through SHM—producing Ig variants, which then compete for limiting T follicular helper (T<sub>FH</sub>) cell survival through coordinated and organized cellular interactions (Cyster and Allen, 2019; Mesin et al., 2016). This competition matures the affinity of the antibodies produced by the B cells and facilitates differentiation of these GC-experienced B cells into long-lived plasma cells



(LLPCs) and memory B cells, necessary cell types for sustained antibody production and efficient cellular recall responses (Balaz et al., 2019; Weisel and Shlomchik, 2017). Memory B cells can more efficiently differentiate into antibody secreting plasma cells upon subsequent pathogen invasion, but pre-formed pathogen-specific antibodies produced from LLPCs represent an additional layer of immune function that can protect from initial invasion. B cells that are activated outside of GCs can also differentiate into memory B cells (Takemori et al., 2014) in addition to shorter-lived versions of antibody-secreting cells such as plasmablasts and short-lived plasma cells (SLPCs).

COVID-19-recovered subjects produce IgGs targeting viral nucleocapsid (N), spike (S), and the S receptor-binding domain (RBD) of spike, which is of particular relevance for their high likelihood of neutralizing capacity (Premkumar et al., 2020). However, these antibodies are low magnitude in the majority of mild SARS-CoV-2 infections, with higher levels produced in more severe disease (Long et al., 2020a; Ma et al., 2020; Wang et al., 2020). These low initial antibodies levels have been shown to decline in most individuals (Beaudoin-Bussi eres et al., 2020; Grandjean et al., 2020; Isho et al., 2020; Iyer et al., 2020; Long et al., 2020b; Seow et al., 2020).

While S-reactive antibodies from convalescent patients can potentially neutralize SARS-CoV-2, they largely lack evidence of SHM (Ju et al., 2020; Robbiani et al., 2020; Rogers et al., 2020). The low SHM in SARS-CoV-2-reactive memory B cells and weak responses hint at low utilization of the GC process, consistent with reports of primarily extrafollicular (i.e., outside GC) immune responses (Woodruff et al., 2020) and dysregulated GC responses (Kaneko et al., 2020) in subjects with severe COVID-19. In this light, whether natural SARS-CoV-2 infection can lead to sustained antibody responses, and what may influence these responses are critical questions.

To address this, we conducted a longitudinal study of COVID-19 convalescent subjects. We quantified plasma IgG and IgM, as well as the stability of plasma IgG to multiple SARS-CoV-2 antigens among subjects with mostly mild disease over time. We found that the anti-SARS-CoV-2 antibodies were broadly distributed and correlated with symptom severity. While a majority displayed IgG decay, a distinct subset showed sustained levels of anti-SARS-CoV-2-specific IgG levels over the same time frame. This distinct subset showed shorter symptom duration, increased SHM in SARS-CoV-2 S-reactive memory B cell antibody genes shortly after symptom resolution, and an increase in frequencies of previously activated CD4<sup>+</sup> T cells. These findings suggest a distinct immunophenotype connecting symptomatic disease resolution kinetics and antibody durability dynamics for SARS-CoV-2.

## RESULTS

### Recruitment and Enrollment

We recruited subjects that recovered from COVID-19 between March 2020 and June 2020 in the Boston, MA area. Each case was diagnosed based on symptoms consistent with COVID-19 and confirmatory laboratory testing (91 PCR test-confirmed and 1 antibody test-confirmed COVID-19) (Table S1). Five individuals were hospitalized, while all others recovered at home

with mostly mild disease. The 1<sup>st</sup> blood sample was collected following primary symptom resolution followed by repeated collections at monthly intervals. Plasma and peripheral blood cells were isolated from each blood sample for analysis.

### Antibody Responses to SARS-CoV-2 Infection Range from Undetectable to Robust

Quantitative ELISA measurement of plasma anti-SARS-CoV-2 IgG and IgM to N, S, and RBD revealed a 3-order magnitude range of virus-specific IgG (Figure 1A). Five of the 92 subjects showed no greater IgG pre-pandemic era controls, consistent with previously reported positivity rates in mild cases (Harritshoej et al., 2020; Hou et al., 2020; Meyer et al., 2020; Rijkers et al., 2020). Additionally, most subjects displayed levels of anti-SARS-CoV-2 IgM close to pre-COVID-19 era control plasma levels (Figure 1B). Spearman rank-order analysis found significant correlations of anti-SARS-CoV-2 IgG magnitude between both age and self-reported symptom severity, with *r* values between 0.31 and 0.41 (Figure 1C) with no correlations between initial virus-specific IgG level and body mass index (BMI) or symptom duration (Figure 1C). Scatterplots for age and severity with antibody magnitude illustrate that these features trend together (Figures 1D–1I). All additional correlation scatterplots and an illustration of the range of symptom severity scores are given in Figure S1. The direct and highly significant correlation of self-reported symptom severity to anti-SARS-CoV-2 IgG magnitude supports the value of self-reported severity as a fair metric between individuals within this cohort as this is an established correlation (Long et al., 2020a; Robbiani et al., 2020).

We also performed Luminex assays to measure reactivity of specific antibody isotypes (including IgM, IgG1, IgG2, IgG3, IgG4, and IgA) to SARS-CoV-2 antigens as well as antibody interactions with Fc receptors (FcRs) (Figure 2). We compared anti-SARS-CoV-2 IgG and IgM levels between pre-pandemic negative control samples and the first 60 recruited subjects from the COVID-19 convalescent cohort (Figures 2A and 2B). The Luminex assay confirmed ELISA-based IgG observations and was superior to ELISA at differentiating the low anti-S IgM levels between controls and SARS-CoV-2 infected individuals (Figure 2B). We observed that 10%–15% of subjects were negative for anti-N, anti-S, and anti-RBD IgG1, consistent with ELISA data (Figure 2C). IgM measurements showed that 20%–49% of COVID-19-recovered subjects could not be distinguished from negative controls by the time of the 1<sup>st</sup> blood draw (Figure 2D). Strong correlations between anti-N and anti-S or anti-N and anti-RBD IgG1 levels (Figures 2E and 2F) suggest that some individuals may recover from COVID-19 without measurable antibodies. It is possible these individuals had a false-positive PCR test, but the criteria for the presence of symptoms plus the positive test make false positives less likely.

We used a machine learning latent variable modeling approach to discern covariation features most importantly associated with severity. We separated individuals into low (1–4) or high (5–10) severity groups and performed orthogonal partial least square discriminant analysis (OPLS-DA), in which measurement variance contributing to discrimination between these two categories is accounted for in one latent variable comprising a weighted combination of critical features selected by

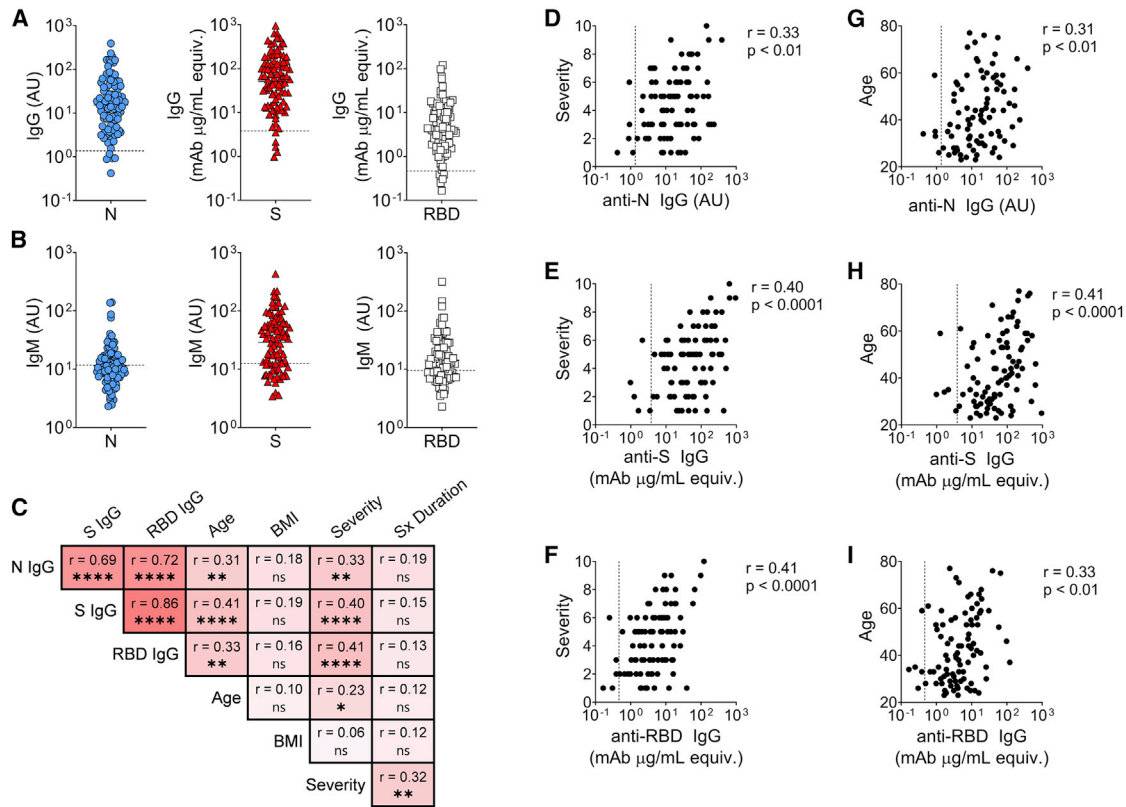


**Figure 1. Humoral Responses to SARS-CoV-2 Antigens Are Broadly Distributed and Correlate with Age and Symptom Severity Among Patients with Mild Disease**

(A and B) Anti-N, anti-S, and anti-RBD IgG (A) and IgM (B) levels for all 92 COVID-19 subjects measured by full titration and comparison to either a pooled plasma standard (AU) or monoclonal antibody standard (mAb  $\mu\text{g}/\text{mL}$  equiv.).

(C) Single variate Spearman correlation matrix displaying  $r$  values and significance levels for correlations between anti-SARS-CoV-2 IgG levels and age, BMI, symptom (Sx) severity, and Sx duration. ns, not significant; \* $p < 0.05$ , \*\* $p < 0.01$ , \*\*\* $p < 0.001$ , and \*\*\*\* $p < 0.0001$ . Surveys were >97% complete for each category. Color indicates strength of positive correlation.

(D–I) The relationships between symptom severity and anti-N (D), anti-S (E), and anti-RBD (F) IgG levels are displayed as scatterplots. Similarly, the correlations between age and anti-N (G), anti-S (H), and anti-RBD (I) IgG levels are given.  $r$  and significance from Spearman correlation are given at the top of the plot. For all plots, the black dashed lines represent twice the average of negative controls.

regularization from the Luminex and ELISA data (Figure 2G). The result suggests that anti-S1 IgG1, anti-RBD IgG titer, anti-N IgG2, and IgG3 measures are most importantly correlative of high symptom severity (Figure 2H). This model is 65% accurate at predicting symptom severity based on an area under the curve of the receiver-operator characteristic (ROC) curve analysis (Figure 2I). Correlation network analysis (Figure 2J) illustrates the additional antibody features that covary with the four key features, representing the most germane immune system processes more broadly. The Luminex assay also included influenza hemagglutinin (HA) and S RBDs from three cold-causing coronaviruses. Antibodies to these antigens generally did not predict COVID-19 disease outcomes (Figure S2), although IgG to human coronavirus 229E did associate with COVID-19 symptom severity.

### Dynamics of Anti-SARS-CoV-2 IgG over 3 Months

We explored antibody decay dynamics by quantifying anti-N, anti-S, and anti-RBD IgG for repeated plasma isolations (Fig-

ure 3). Seventy-six subjects donated 2<sup>nd</sup> and 3<sup>rd</sup> monthly samples (median 39, range 13–88) such that draw 3 was  $\sim 100$  days following disease onset (median 109, range 83–173) (Figure 3A). Virus-specific IgG decline occurred in most individuals. We quantified this decline by calculating the quotient of the 3<sup>rd</sup> draw IgG level divided by the 1<sup>st</sup> draw IgG level for each antigen and deemed this the “antibody durability index” (Figure 3B). Anti-N IgG declined in 88%, anti-S in 72%, and anti-RBD in 74% of the convalescent subjects by their 3<sup>rd</sup> blood draw. The median antibody durability index values were 0.49, 0.65, and 0.61 for anti-N, anti-S, and anti-RBD IgG, respectively. These findings are consistent with a decaying IgG response in the majority of COVID-19 convalescent subjects.

While the majority of convalescent subjects showed decline, some individuals showed stable or enhanced antibody production over the same time period. We examined this by grouping subjects based on their  $\sim 100$ -day (i.e., draw 3-defined) antibody durability indices into “sustainer” (durability index  $\geq 1$ ) and “decayer” (durability index  $< 1$ ) categories. We noted that

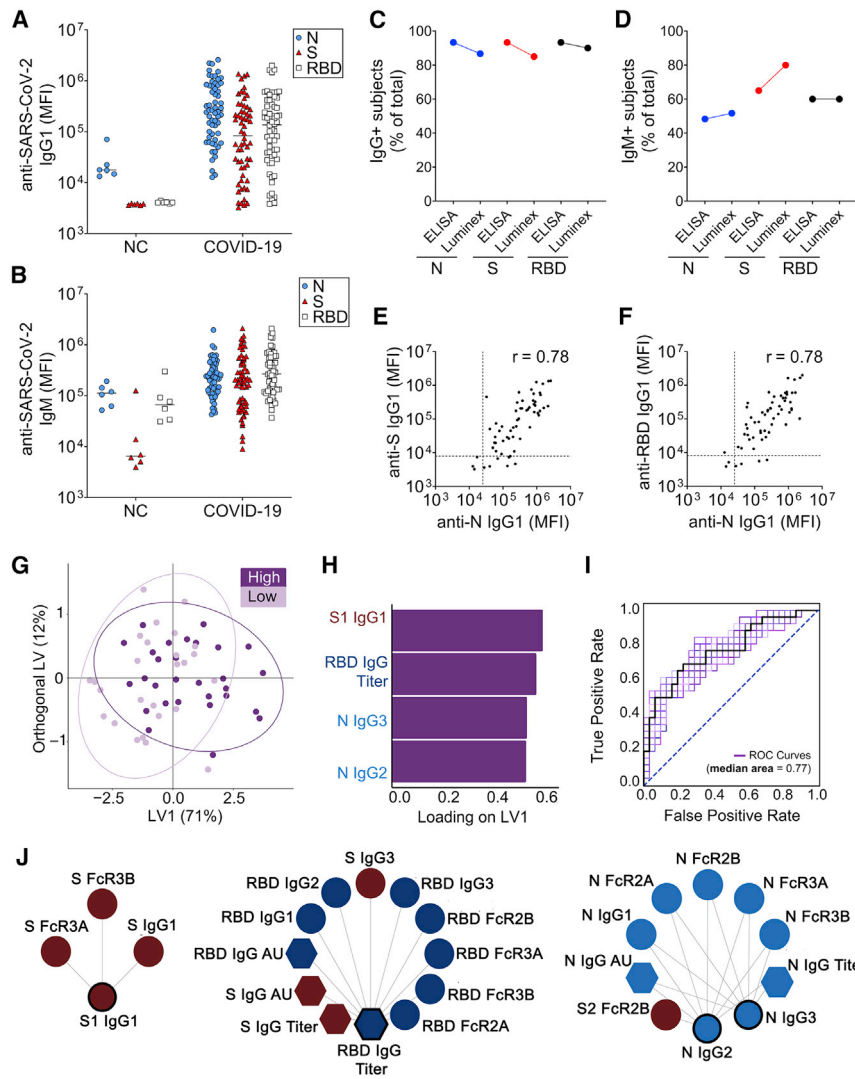


**Figure 2. Luminex Analysis of COVID-19 Samples Confirms that the Plasma Antibody Response to SARS-CoV-2 Infection Ranges from Robust to Negligible**

(A and B) IgG1 (A) and IgM (B) reactivities to N (blue circles), S (red triangles), and RBD (white squares) as measured by Luminex among pre-pandemic (negative control) samples (NC, n = 6) and a subset of the COVID-19 convalescent cohort (COVID-19, n = 60).

(C and D) Plots showing the proportions of the COVID-19 subjects analyzed by Luminex and ELISA that are positive for anti-N (blue), anti-S (red), and anti-RBD (black) antibody. IgG (ELISA)/IgG1 (Luminex) (C) and IgM (D) are shown. Positivity cut off was set at twice the average signal of the negative control samples.

(E and F) Scatterplots showing the correspondence between the anti-N and anti-S IgG1 (E) and anti-N and anti-RBD IgG1 (F) Luminex values. Black dashed lines represent twice the average of negative controls and Spearman r value for the correlation is shown.

(G) Latent variable scores biplot resulting from orthogonal partial least square discriminant analysis (OPLS-DA) with symptom severity as outcome variable. Each point is an individual patient, colored by symptom severity. Ellipses illustrate the 95% confidence intervals for each outcome.

(H) Loadings plot depicting feature importance on the 1<sup>st</sup> latent variable. Feature names are colored by antigen (N: light blue; S: red; RBD: navy). Bar color corresponds with the symptom severity group that the feature correlates most highly with based on median feature values.

(I) OPLSDA model performance. ROC curves (purple) for 100 5-fold cross validated trials predicting symptom severity based on the OPLS-DA model. The median AUC score is labeled in the legend and the corresponding curve is highlighted in black. Blue dashed line denotes classification threshold for a random process.

(J) Correlation networks identifying ELISA (hexagon) and Luminex (circle) features that co-correlate with the four features selected for the OPLS-DA model (outlined in black). Edges exist between features with correlation strength greater than 0.75 and  $p < 0.01$ . Nodes are colored by antigen as in (H).

most individuals qualifying as IgG sustainers with respect to one antigen also sustained production of IgG specific to the other antigens (Figure 3C; Table S2). Plotting quantitative (Figure 3D) as well as draw 1-normalized (Figure 3E) antibody levels over the first three blood draws showed the trend of stable/increasing antibody levels in sustainers and decreasing antibody levels in decayers. Plotting the same data as days post symptom onset demonstrated a similar diversity of timing of blood draws between the groups (Figures S3A and S3B). In addition, sustainers and decayers do not differ substantially in timing of blood draws, either with respect to symptom onset or symptom resolution (Figures S3C–S3F).

### Rapid Resolution of COVID-19 Symptoms Correlates with Sustained Antibody Production

Of the 76 individuals who completed three longitudinal blood draws, 72 seroconverted. For these 72 individuals, we explored

associations between subject and disease characteristics and sustained antibody production (Figure 3F) using Spearman correlation analysis. Both anti-S and anti-RBD IgG durability indices significantly correlated inversely with disease symptom duration, with r values of  $-0.28$  and  $-0.27$ , respectively. The anti-N IgG durability index showed no significant relationship with symptom duration, suggesting a unique effect of the anti-S and anti-RBD antibodies. Full scatterplots for the correlation between anti-S (Figure 3G) and anti-RBD (Figure 3H) durability indices and COVID-19 symptom duration illustrate the association between a shorter disease course and more durable antibody responses. Anti-S IgG durability also correlated inversely with symptom severity ( $r = -0.27$ ). No significant correlations were found between age or BMI and antibody durability (Figures 3F and S4A–S4S).

Direct comparison of symptom duration showed that anti-S IgG sustainers had significantly shorter symptom duration

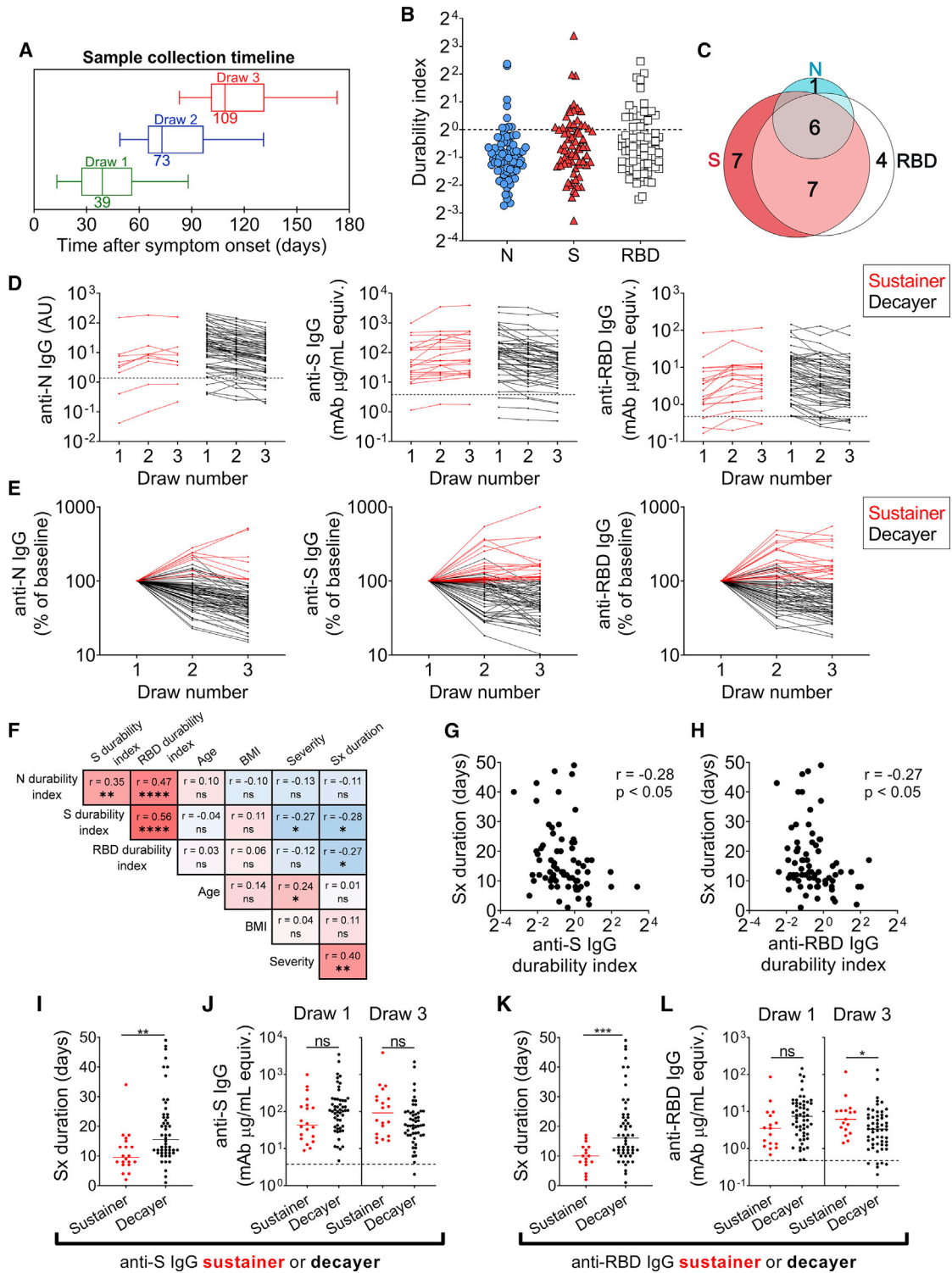


**Figure 3. Longitudinal Plasma Samples Define a Subset of Swift-Healing Subjects with Stable or Increasing Anti-SARS CoV-2 Ig Levels at ~100 Days after Symptom Onset**

(A) Box and whisker plots illustrating blood draw schedule with medians indicated.

(B) Plot showing the ranges of antibody durability indices for subjects that donated three blood samples ( $n = 76$ ). The durability index for each antigen here is the quotient of the 3<sup>rd</sup> blood draw IgG level divided by the first blood draw from the same individual. Dashed line at unity.

(C) Venn diagram illustrating overlap between anti-N, anti-S, and anti-RBD sustainer groups.

(legend continued on next page)

(median 9.5, range 2–34) than anti-S IgG decayers (median 15.5, range 1–49) (Figures 3I and 3K). Anti-RBD IgG sustainers also had significantly shorter symptom duration (median 10, range 2–17) compared to anti-RBD IgG decayers (median 16, range 1–49). Similar analyses for age, BMI, and symptom severity did not reveal significant differences (Figures S4T and S4U). Anti-S IgG and anti-RBD IgG sustainers had draw 1 anti-S IgG and anti-RBD IgG spanning the range of levels observed for the entire cohort (Figures 3D and S4V). In addition, direct comparisons of initial antibody levels among sustainers and decayers showed no significant differences (Figures 3J and 3L), and we saw no significant relationship between initial IgG level to N, S, or RBD and disease symptom duration (Figure 1C). Despite similar initial blood draw levels, sustainers showed a trend toward greater anti-S IgG (Figure 3J) and significantly more anti-RBD IgG (Figure 3L) compared to decayers in draw 3, consistent with the notion that a unique feature of sustainers is anti-virus IgG maintenance in contrast to initial magnitude. Together, these data indicate that relatively sustained antibody production occurs within individuals with a diverse range of initial IgG magnitude and shortened disease course.

While it is unknown what level of measurable functional antibody activity correlates with protection, we explored potential functional consequences of differences in antibody decay dynamics between draw 1 and 3 (Figure S5). A major mechanism of antibody neutralization of SARS-CoV-2 is inhibition of binding of S to angiotensin-converting enzyme 2 (ACE2), the receptor for SARS-CoV-2 (Hoffmann et al., 2020). ACE2-binding inhibition assays showed that while initial inhibition activity was lower for sustainers than decayers, they became indistinguishable by draw 3 (Figures S5A and S5B). Relatedly, sustainers had higher ACE2-inhibition durability indices (Figures S5A and S5B), indicating that overall stability of antibody responses correlated with more stable functional activity. We also measured stability of SARS-CoV-2 neutralization activity using an automated high-throughput pseudovirus neutralization assay as well as conventional pseudovirus neutralization assays (Figure S5C). Neutralization titer positively correlated with age and disease severity, similar to overall antibody levels (Figure S5D). In contrast to ELISA antibody measurements and ACE2 inhibition levels, 50% neutralization titers ( $NT_{50}$ ) were tightly clustered among all subjects in the 1<sup>st</sup> and 3<sup>rd</sup> samples with no evidence of differences in magnitude or durability dynamics between sustainers and decayers at these time points (Figures S5F–S5I). The constrained ability to distinguish subjects based on differences

in  $NT_{50}$  levels over time was likely due to the small range of values approaching limit of detection, in contrast to other antibody measures (Figure S5E). In this regard, substantial  $NT_{50}$  decline between draw 1 and draw 3 was observed only within individuals with high initial neutralization titers (Figure S5C).

### Antibody Sustainers Harbor Reduced Naive CD4<sup>+</sup> T Cells and Increased Memory B Cell SHM

To further explore features of the swift-healing antibody-sustainer phenotype, we characterized CD4<sup>+</sup> (Figure 4) and CD8<sup>+</sup> (Figure S6) T cell populations using a previously established T cell phenotyping strategy (Mathew et al., 2020). We observed that sustainers had a higher frequency of memory (CD45RA<sup>-</sup>) CD4<sup>+</sup> T cells in both 1<sup>st</sup> draw and in their 3<sup>rd</sup> draw several months later. No significant differences in CD8<sup>+</sup> T cell populations were observed. These data suggest that those that heal quickly from mild COVID-19 harbor differences in CD4<sup>+</sup> T cell subsets that persist well past disease resolution.

We also fluorescence-activated cell sorting (FACS)-sorted S-specific single memory B cells and sequenced their Ig genes to assess SHM. We confirmed that S-specific memory cells were not plasmablasts based on CD20 and CD38 expression (Figures S7A–S7C). We selected 12 sustainers and 13 decayers based on similar initial antibody levels (Figures S7J and S7K). Clinical and antibody features of these subjects showed they are representative of each group (Figures S7D–S7Q), and they had similar frequencies of S-specific memory cells (Figures 5A and 5B). We observed significantly higher IgH V gene segment ( $V_H$ ) mutations in the sustainer clones isolated from the 1<sup>st</sup> blood draw (Figure 5C). We found that 19.4% of draw 1 sustainer clones had greater than 15 mutations (top 10<sup>th</sup> percentile) in contrast to 4.2% of decayer clones (Figure 5D). We also found that sustainer-derived clones with less than 15 mutations also had significantly higher draw 1 mutation frequency (Figure S7R). The difference in mutation frequency between sustainers and decayers collapsed by the time of the 3<sup>rd</sup> blood draw (Figures 5C and 5D) as both groups gained significantly more mutations by draw 3. Light chain V gene ( $V_L$ ) mutation largely paralleled the  $V_H$  results (Figures 5E and 5F). No differences in  $V_H$  gene segment usage were observed between the groups (Figure 6G). These data suggest that increased virus-specific memory B cell SHM early after recovery may be a unique sustainer feature and that continued evolution of anti-SARS-CoV-2 memory B cells occurs more globally later on in convalescence.

(D and E) Subjects were grouped as either having stable or decaying antibody levels based on their antibody durability index, with “sustainers” (red)  $\geq 1$  and “decayers” (black)  $< 1$ . The changes in anti-N (left), anti-S (middle), and anti-RBD (right) IgG levels across draws are expressed as an absolute value (D) or relative to the value for that subject in draw 1 (baseline) (E).

(F) Single variate Spearman correlation matrix displaying  $r$  values and significance levels for correlations between antibody durability indices and the indicated variables derived from survey data ( $n = 72$ ). Survey data were complete for all categories excluding BMI, for which one subject declined to provide data.

(G and H) Scatterplots illustrating the correlations between the anti-S (G) and anti-RBD durability index (H) and duration of COVID-19 symptoms, with  $r$  and significance from Spearman correlation analysis.

(I–L) Comparison of symptom duration reported for individuals with stable anti-S IgG levels (I) and anti-RBD IgG levels (K) (sustainers, red;  $n = 20$  and  $n = 17$ , respectively) to those with decaying levels (decayers, black;  $n = 52$  and  $n = 55$ , respectively). Comparisons of draw 1 and draw 3 IgG antibody levels among anti-S (J) and anti-RBD (L) IgG sustainers and decliners shown in (I and K). Horizontal lines indicate medians.

For (D), (J), and (L), black dashed lines represent twice the average of negative controls. Student's  $t$  test was used for significance testing of differences in antibody levels following a log transformation of the values. Significance testing for differences in symptom duration used the Mann-Whitney U test. ns, not significant. \* $p < 0.05$ , \*\* $p < 0.01$ , \*\*\* $p < 0.001$ .

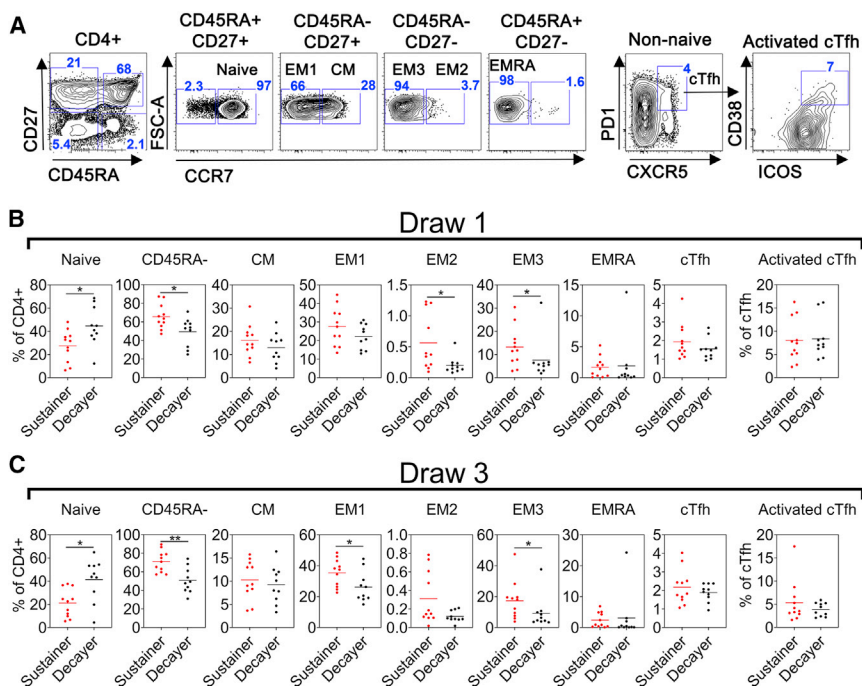


**Figure 4. Naive CD4<sup>+</sup> T Cells Are Reduced in Sustainers**

(A) Representative flow plots illustrating the gating strategy used to define the CD4<sup>+</sup> T cell (CD3<sup>+</sup>CD8<sup>-</sup>CD4<sup>+</sup>) populations measured, including naive (CD45RA<sup>+</sup>CD27<sup>+</sup>CCR7<sup>+</sup>), central memory (CM, CD45RA<sup>-</sup>CD27<sup>+</sup>CCR7<sup>+</sup>), effector memory 1 (EM1, CD45RA<sup>-</sup>CD27<sup>+</sup>CCR7<sup>-</sup>), effector memory 2 (EM2, CD45RA<sup>-</sup>CD27<sup>-</sup>CCR7<sup>-</sup>), effector memory 3 (EM3, CD45RA<sup>-</sup>CD27<sup>-</sup>CCR7<sup>-</sup>), CD45RA<sup>+</sup> effector memory (EMRA, CD45RA<sup>+</sup>CD27<sup>-</sup>CCR7<sup>-</sup>), circulating Tfh (cTfh, CD45RA<sup>-</sup>PD1<sup>+</sup>CXCR5<sup>+</sup>), and activated cTfh (CD45RA<sup>-</sup>PD1<sup>+</sup>CXCR5<sup>+</sup>CD38<sup>+</sup>ICOS<sup>+</sup>).

(B and C) Quantification of the CD4<sup>+</sup> T cell populations among PBMCs from sustainers (n = 11) and decayers (n = 10) in draw 1 (B) and draw 3 (C). Means are represented as horizontal lines in the plots. Mann-Whitney U test. \*p < 0.05, \*\*p < 0.01.

### Sustained Virus-Specific IgG Production at ~100 Days Predicts Antibody Persistence at ~145 Days

Sixty-eight subjects returned for a 4<sup>th</sup> blood draw, of which 64 showed SARS-CoV-2 seroconversion (Figure 6). The 4<sup>th</sup> draw samples allowed us to test whether (1) antibodies remain durable in sustainers and (2) whether this durability translates to greater antibody levels at ~145 post symptom onset (Figure 6A). For this analysis, we continued to divide subjects based on their antibody durability index calculated for blood draw 3 (i.e., draw 3-defined sustainers and decayers) (Figure 6B) and measured overall antibody levels, ACE2 binding inhibition, and pseudovirus neutralization for the 4<sup>th</sup> draw blood samples (Figures 6C and 6D). For these draw 3-defined groups, we calculated draw 4 durability indices by dividing a subject's 4<sup>th</sup> draw value by their 1<sup>st</sup> draw measure. After a relatively short period of ~1 month between draws 3 and 4, absolute magnitudes of anti-S and anti-RBD IgG had become significantly greater for sustainers compared to decayers. The total antibody durability indices were also significantly higher for sustainers compared to decayers. Additionally, anti-S IgG sustainers had significantly greater neutralizing antibody at this time point (Figure 6C) and anti-S and anti-RBD sustainers showed significantly higher ACE2 binding inhibition durability indices in draw 4.

We reanalyzed our cohort by grouping subjects as sustainers or decayers based on ratios of draw 4 IgG levels to those in draw 1 (i.e., draw 4-defined sustainers and decayers) to compare to draw 3-defined groups (Figure 7A). We found considerable overlap in draw 3- and draw 4-defined sustainers (Figure 7B). The key clinical correlation—reduced symptom duration in sustainers—was also observed for draw 4-defined sustainers (Figures 7C and 7D). We also observed similar differences in total antibody levels and neutralization and durability indices for draw

4-defined sustainers (Figures 7E and 7F) as we did for draw 3-defined sustainers (Figures 6C and 6D). Together, these data strengthen the conclusion that sustained production of virus-specific IgG is associated with short disease duration. The data also indicate that despite a large range of initial antibody levels, IgG sustainers end up having greater antibody magnitudes compared to decayers as a whole.

## DISCUSSION

The data presented here show that antibody responses to SARS-CoV-2 in mild disease are broadly distributed following infection and declined substantially in most individuals over time. However, some individuals sustained antibody levels over the same time frame. These IgG sustainers had shorter disease courses despite similar distribution of initial anti-SARS-CoV-2 IgG levels, and their anti-S memory B cells harbored increased levels of SHM shortly after disease resolution. Heterogeneity of sustained and declining antibody titers has been documented in common cold coronaviruses. A small study showed that some individuals after virus challenge produced near peak levels of anti-coronavirus IgG 50 weeks out from virus challenge, while others declined near background signal levels between 10 and 20 weeks (Callow et al., 1990). A lack of sustained immunity to seasonal coronaviruses has also been shown epidemiologically (Edridge et al., 2020; Kiyuka et al., 2018). While antibody durability is known to be influenced by virus type (Amanna et al., 2007) as well as host and environmental factors (Hagan et al., 2019), why certain individuals produce longer-lived antibody responses while others do not is not fully understood.

Anti-SARS-CoV-2 antibody decline toward baseline as seen in many individuals is consistent with a dominant role for short-lived plasmablasts and/or SLPCs as a transient antibody source. This, paired with low disease-proximal memory B cell SHM in most individuals, is consistent with dominant extrafollicular antibody responses in IgG decayers (Woodruff et al., 2020) perhaps

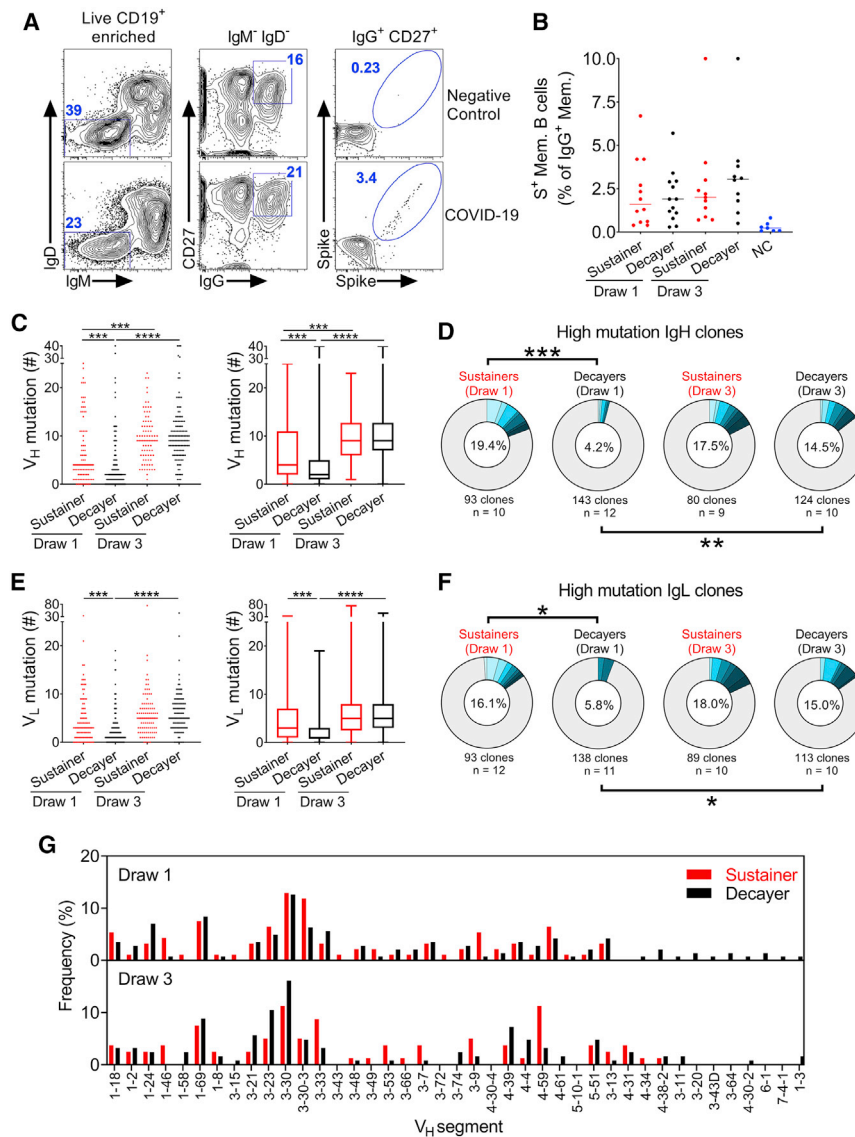


**Figure 5. Increased Early SHM in S-Specific Memory B Cells from Sustainers**

(A) Cytometric gating strategy for anti-SARS-CoV-2 S-specific IgG memory B cell (IgG Mem. B cells, DAPI<sup>-</sup>CD19<sup>+</sup>IgM<sup>-</sup>IgD<sup>-</sup>IgG<sup>+</sup>CD27<sup>+</sup>Spike<sup>+</sup>) sorting from CD19<sup>+</sup> enriched PBMCs from a representative negative control subject (top) and a COVID-19 convalescent subject (bottom). Sequential gating events are shown left to right.

(B) Summary data for the percent of S<sup>+</sup> IgG memory B cells among IgG<sup>+</sup> memory cells from draws 1 and 3 of sustainers (red, draw 1: n = 12 and draw 3: n = 11) and decayers (black, draw 1: n = 13 and draw 3: n = 10). Kruskal-Wallis test showed no significant differences.

(C) Dot plots (left) and box and whisker plots (right) showing mutation numbers per sequence in the heavy chain V gene segment (V<sub>H</sub>) of sorted S<sup>+</sup> single memory B cells from sustainers and decayers. For draw 1, 93 productive clones were obtained from 10 sustainers and 143 productive clones from 12 decayers. For draw 3, 80 productive clones were obtained from 9 sustainers and 124 productive clones from 10 decayers. Kruskal-Wallis test.

(D) Donut charts illustrating percent of V<sub>H</sub> sequences in (C) with <15 mutation (gray) or ≥15 mutation (shades of blue) for sustainers and decayers. Fifteen represents the 90<sup>th</sup> percentile for V<sub>H</sub> mutation distribution. Shades of blue represent sequences contributed by a single subject. Fisher's exact test.

(E) Analysis of mutation frequency in light chain V gene segments (V<sub>L</sub>) as described for V<sub>H</sub> in (C). Draw 1 includes 93 productive clones from sustainers and 138 from decayers. Draw 3 includes 89 productive clones from sustainers and 113 from decayers.

(F) Donut charts illustrating the percent of V<sub>L</sub> sequences in (E) with <10 mutation (gray) or ≥10 mutation (shades of blue) for sustainers and decayers. Ten represents the 90<sup>th</sup> percentile for V<sub>L</sub> mutation distribution. Shades of blue represent sequences contributed by a single subject. Fisher's exact test.

(G) V gene segment usage among all analyzed heavy chain clones for sustainers (red bars) and decayers (black bars) in draw 1 (top) and draw 3 (bottom). Medians are represented as horizontal lines.

For (A–G), ns, not significant; \*p < 0.05, \*\*p < 0.01, \*\*\*p < 0.001, and \*\*\*\*p < 0.0001.

due to impaired GCs as seen in individuals with more severe disease (Kaneko et al., 2020). Why SARS-CoV-2 infection may be associated with predominantly extrafollicular antibody responses and dysregulated GCs remains to be fully elucidated. It is possible that the same pro-inflammatory mediators contributed by innate and adaptive immune cells that drive severe disease in some cases (Lucas et al., 2020) are the same that dysregulate the GC processes as has been shown in severe malaria (Ryg-Cornejo et al., 2016) and intracellular bacterial infections (Popescu et al., 2019). A similar process could underlie GC inhibition in severe COVID-19 (Kaneko et al., 2020) and may underlie declining antibody levels due to largely extrafollicular B cell activation and/or suboptimal GC responses in most individuals with mild COVID-19 as well.

Low SHM antibodies can be potent neutralizers (Ju et al., 2020; Robbani et al., 2020; Rogers et al., 2020), suggesting that the human pre-immune antibody repertoire is not deficient in specificities to neutralizing targets on SARS-CoV-2 spike (Brouwer et al., 2020). SARS-CoV-2 humoral responses are therefore not constrained by gaps in the repertoire but may be limited by poor mobilization of B cells into the LLPC compartment to produce high titer sustained responses as can be seen in other infections (Amanna et al., 2007), consistent with potential suppression of optimal GC responses and LLPC differentiation in COVID-19. Notably, SHM levels among sustainer and decayer memory B cells continue to accumulate SHM several months following resolution of infection consistent with recent work showing increased plasma avidity to SARS-CoV-2 in

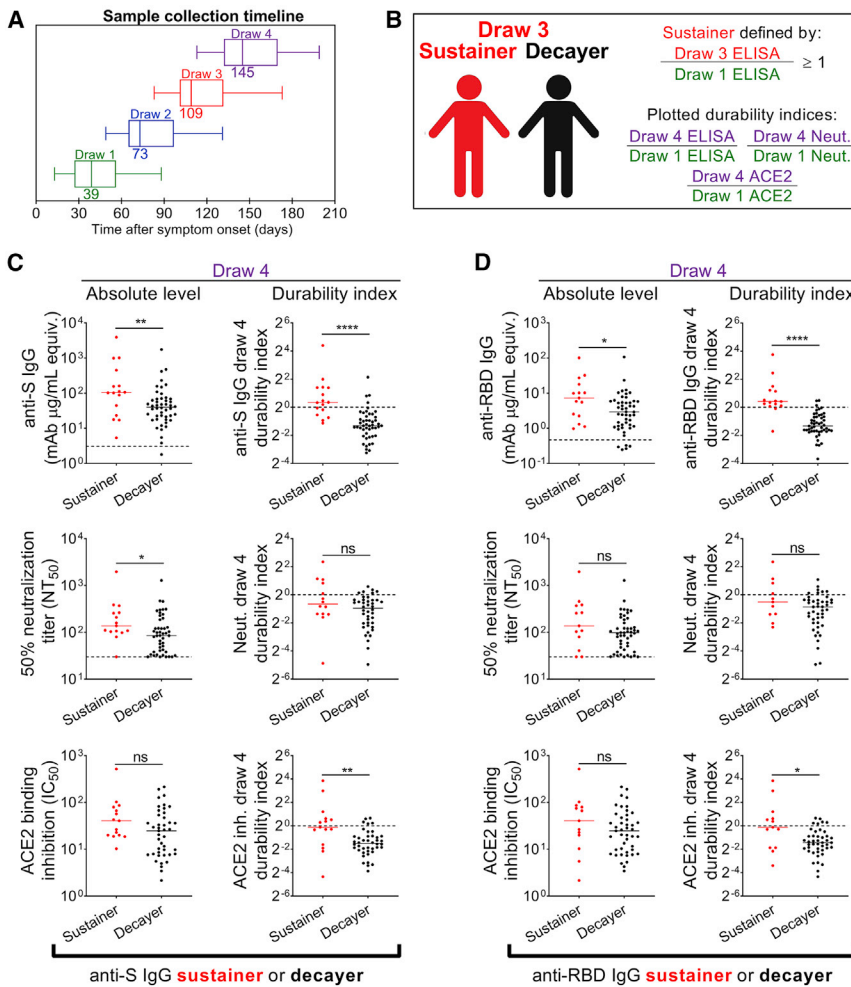


**Figure 6. Individuals with Stable Antibody at ~100 Days Maintain Antibody Levels at ~145 Days**

(A) Blood collection timeline as in Figure 3A, with the addition of the 4<sup>th</sup> blood draw plot (purple, n = 68).

(B) Analysis strategy in this figure. Draw 4 durability index analysis for subjects grouped by draw 3-defined antibody durability indices.

(C) Plots comparing the magnitudes (left) and durability (right) of total anti-SARS-CoV-2 IgGs (top), pseudovirus neutralization titers (middle), and ACE2 binding inhibition titers (bottom) for draw 3-defined anti-S IgG sustainers and decayers (n = 16 sustainers and n = 48 decayers). Dashed lines for total antibody levels represent the positivity cutoff described above and the limit of neutralization detection.

(D) Plots are as described for (C), with draw 3-defined anti-RBD IgG sustainers (n = 15) and decayers (n = 49). Student's t test was used for significance testing of differences in total antibody levels following a log transformation. All other significance testing used the Mann-Whitney U test. ns, not significant; \*p < 0.05, \*\*p < 0.01, \*\*\*p < 0.001, and \*\*\*\*p < 0.0001. Horizontal lines indicate medians.

production adds support to a distinct immunophenotype connected to more rapid resolution of disease. Whether the increased percentage of effector memory T cells in sustainers is a reflection of increased disposition to CD4<sup>+</sup> effector memory differentiation, an indicator of past experience, or whether it is related to COVID-19 sequelae in sustainers remains to be uncovered.

convalescent individuals over time (Piccoli et al., 2020). Antigen from pathogens can be retained for many months by follicular dendritic cells in secondary lymphoid tissues allowing affinity maturation to proceed in the absence of an active infection. It is possible that a return to a normal inflammatory milieu after resolution of COVID-19 restores GCs that may have been suppressed only during active disease, and selection on retained viral antigen facilitates late accumulation of SHM in decayers. A non-mutually exclusive alternative is that memory B cells that lack SHM may be counter-selected over time independent of continued GC output (Takahashi et al., 1998).

An important implication of our data is the possible existence of an efficient SARS-CoV-2 virus “handler” phenotype, defined as individuals who experience swift COVID-19 resolution associated with relatively sustained anti-SARS-CoV-2 IgG production. Based on the requirement of GCs for LLPCs and SHM accumulation, this suggests that the sustainer phenotype may include relatively more optimal coordination of lymphocyte interactions in physiologic GC responses. In this regard, GC dysregulation and short-lived antibody responses may not be inevitable outcomes of COVID-19. Elevated percentages of CD4<sup>+</sup> effector memory T cells in those that heal quickly and sustain antibody

The degree to which the efficient healer phenotype is due to intrinsic host differences or prior immune priming also warrants further investigation. Sustainers could represent a subset of individuals with pre-existing memory lymphocytes from a seasonal coronavirus infection that happens to cross-react with SARS-CoV-2. Reactivation of cross-reactive memory cells could prime GC reactions for more optimal function and a recall response may help explain the limited disease duration of sustainers. It is also possible that stimulation of pre-existing memory B cells in this context may be more prone to generate LLPCs. This scenario would also be consistent with the observation of higher early SHM levels in sustainers compared to decayers. Arguing against a priming model is that analysis of other human coronaviruses did not show correlations with COVID-19 symptom duration. However, because timing of potential priming events may matter, and antibodies to common human coronaviruses may not be sustained, analysis beyond antibody levels will be required to further address this.

As discussed above, increased SHM does not appear to be required for potent anti-SARS-CoV-2 antibody neutralization function. In this light, we think it unlikely that the elevated early SHM in

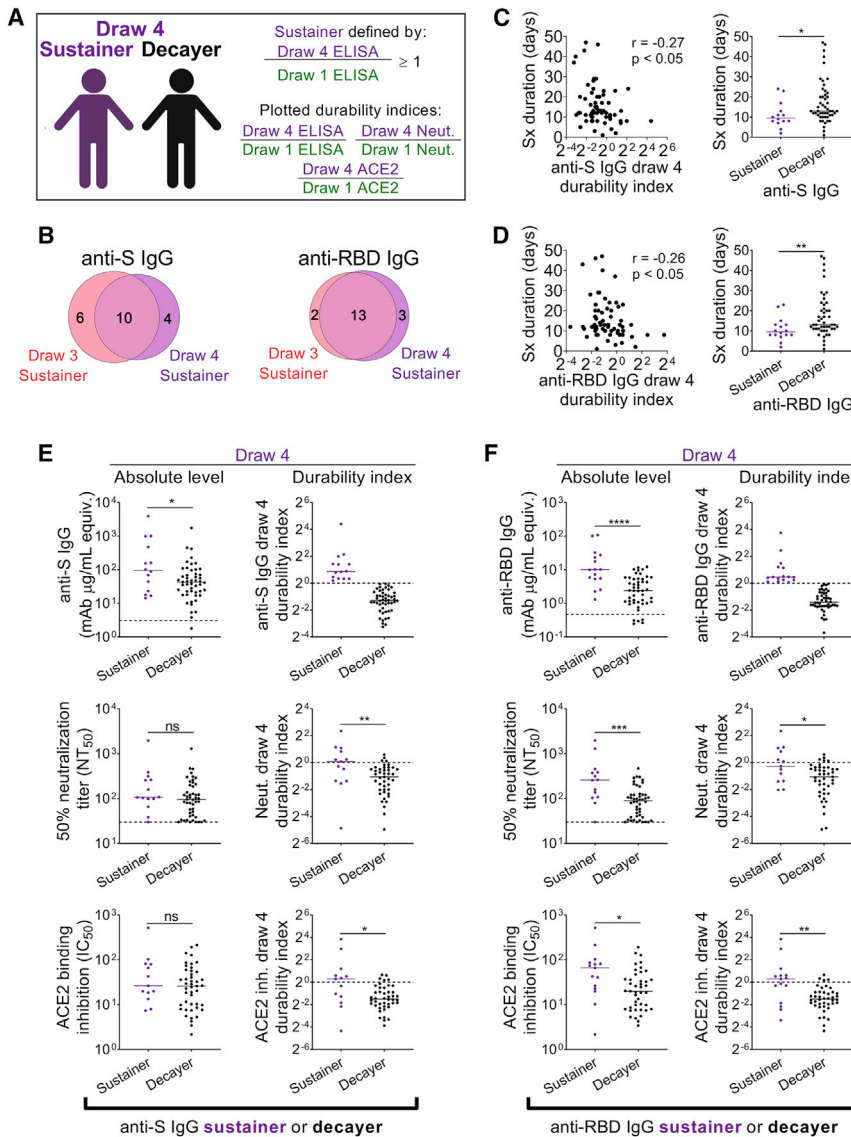


**Figure 7. Reanalysis Using 4<sup>th</sup> Draw Durability Indices Confirms that Sustained Antibody Production Correlates with Reduced Symptom Duration**

(A) Analysis strategy in this figure. Subjects are grouped based on their 4<sup>th</sup> draw antibody durability indices and analyzed based on 4<sup>th</sup> draw antibody measures.

(B) Venn diagram illustrating the overlap between draw 3-defined and draw 4-defined sustainer groups by anti-S IgG durability indices (left) or anti-RBD durability indices (right).

(C) Scatterplots illustrating the correlations between the 4<sup>th</sup> draw anti-S durability index and the duration of COVID-19 symptoms, with *r* and significance from Spearman correlation. A dot plot comparing symptom duration between draw 4 anti-S IgG sustainers (*n* = 14) and decayers (*n* = 50) is given on the right.

(D) Plots as in (C) with draw 4-defined anti-RBD IgG durability for sustainers (*n* = 16) and decayers (*n* = 48).

(E) Plots comparing the magnitudes (left) and durability (right) of total anti-SARS-CoV-2 IgGs (top), pseudovirus neutralization titers (middle), and ACE2 binding inhibition titers (bottom) for sustainers and decayers as defined by draw 4 anti-S IgG. Dashed lines for total antibody levels represent the positivity cutoff described above and for neutralization the limit of detection.

(F) Plots as described for (E), with sustainers and decayers as defined by draw 4 anti-RBD IgG. Student's *t* test was used for significance testing of differences in total antibody levels following a log transformation of the values. All other significance testing for differences in symptom duration used the Mann-Whitney U test. ns, not significant; \**p* < 0.05, \*\**p* < 0.01, \*\*\**p* < 0.001, and \*\*\*\**p* < 0.0001. Horizontal lines indicate medians.

sustainers had a direct causal role in quicker symptom clearance, although we have not ruled this out. Instead, we propose that elevated SHM and durable antibody production in sustainers are sequelae of a superior wholistic immune process that overall was responsible for swifter healing. As a part of the immune process in sustainers, we posit that reduced suppression of optimal GC responses occurred during the original infection resulting in superior LLPC differentiation. Why sustainers heal more quickly and whether this is related to why they were able to sustain virus-specific IgG production, potentially by shielding GCs from infection-mediated dysregulation/suppression, remain to be determined. Understanding the specific drivers of diminished versus enhanced antibody durability in cohorts such as this may provide insights into correlates of protection to SARS-CoV-2 and may elucidate targetable pathways to enhance efficient clearance and more sustained antibody-mediated protection.

**Limitations of Study**

While population diversity was our aim, most volunteers for this study were adults, female, and Caucasian. While we have confidence in the biologic conclusions, it will be important for future studies to understand the nature of antibody responses in children and adults from a diversity of backgrounds and races. In addition, while the mild and moderate cases represented a large portion of SARS-CoV-2 symptomatology (Oran and Topol, 2020; Wu and McGoogan, 2020), severe and asymptomatic cases are not represented here. In this context, our work may also provide a framework to address whether the features of increased SHM coupled with quicker symptom resolution and relatively sustained anti-SARS-CoV-2 antibody responses are seen in severe and asymptomatic cases and whether this extends to seasonal coronavirus biology. Whether continued virus replication plays a role in driving sustained responses also remains to be

determined, but we feel this is less likely as it does not easily explain the quick healing correlate. In addition, future work will be enhanced by including sample collection before and during COVID-19 allowing direct insights into pre-immune correlates of the sustainer and decayer phenotypes.

## STAR★METHODS

Detailed methods are provided in the online version of this paper and include the following:

- **KEY RESOURCES TABLE**
- **RESOURCE AVAILABILITY**
  - Lead Contact
  - Materials Availability
  - Data and Code Availability
- **EXPERIMENTAL MODEL AND SUBJECT DETAILS**
  - Human study participants
- **METHOD DETAILS**
  - ELISA
  - Luminex assay
  - Multi-variate analysis of symptom severity
  - FACS sorting and monoclonal antibody sequence isolation from memory B cells
  - ACE2-binding inhibition assay
  - Conventional SARS-CoV-2 pseudovirus neutralization assay
  - High-throughput SARS-CoV-2 pseudovirus neutralization assay
- **QUANTIFICATION AND STATISTICAL ANALYSIS**

## SUPPLEMENTAL INFORMATION

Supplemental Information can be found online at <https://doi.org/10.1016/j.cell.2020.10.051>.

## ACKNOWLEDGMENTS

We thank study volunteers. This study was supported by NIH grants (T32 AI007245 to J.F., T32 GM007753 to B.M.H. and T.M.C., AI146779 to A.G.S., AI007306 to J.M., AI007512 to A.Z., T32 AI007306 to Y. Chen, AI142790 to D.A.L. and K.M.P., DP2DA040254 and NIDA Avenir Award to A.B.B. and K.M.P., and AI121394, AI139538, AI137940 to D.R.W.). D.R.W. was also supported by the Burroughs Wellcome Fund, Food Allergy Science Initiative, and Massachusetts Institute of Technology Center for Microbiome Informatics and Therapeutics. A.B.B. is supported by an MGH Transformative Scholars Program. K.M.P. is supported by the National Science Foundation Graduate Research Fellowship (#1745302). Grant support was provided by Massachusetts Consortium on Pathogenesis Readiness to A.G.S., B.C., G.A., and D.R.W. and Fast Grant funding for COVID-19 science (to D.R.W.). Support was provided by the Ragon Institute and the Mark and Lisa Schwartz and the Schwartz Family Foundation. Enid Schwartz is also acknowledged. We thank Sudeshna Fisch and Reem Abbaker for support in patient recruitment and sample collection and Losyev Grigoriy for flow cytometry cell sorting. We thank Noah B. Whiteman and Bruce D. Walker for manuscript review. Graphical abstract generated with [BioRender.com](https://www.biorender.com).

## AUTHOR CONTRIBUTIONS

D.R.W. designed the study. Y. Chen and A.Z. conducted ELISA and FACS experiments. S.F. and C.A. conducted Luminex experiments. Y. Chen, A.Z., S.F., C.A., J.M., P.T., D.A.L., K.M.P., G.A., and D.R.W. analyzed data. J.M. and H.M.

assisted with recruitment of the clinical cohort and contributed to writing the paper. S.H., M.T., F.J.N.L., and A.G. recruited patients and processed samples. J.B. and D.G. assisted with clinic study management and sample collection. A.Z., Y. Chen, P.T., A.G., and M.T. did the single-cell sorting and antibody cloning. Y. Chen performed SHM analysis. P.T., A.Z., M.T., A.B.B., M.S.S., C.L.L., and E.C.L. performed neutralization assays and analysis. B.M.H., T.M.C., J.S.B., J.F., A.G.S., Y. Cai, and B.C. contributed recombinant protein. D.A.L. and K.M.P. analyzed data. J.A.L. supplied control plasma samples. A.Z. prepared the first draft. A.Z., Y. Chen, and D.R.W. wrote the paper.

## DECLARATION OF INTERESTS

The authors declare no competing interests.

Received: July 20, 2020

Revised: August 28, 2020

Accepted: October 29, 2020

Published: November 3, 2020

## REFERENCES

- Amanna, I.J., Carlson, N.E., and Slifka, M.K. (2007). Duration of humoral immunity to common viral and vaccine antigens. *N. Engl. J. Med.* **357**, 1903–1915.
- Balaz, M., Becker, A.S., Balazova, L., Straub, L., Muller, J., Gashi, G., Maushart, C.I., Sun, W., Dong, H., Moser, C., et al. (2019). Inhibition of Mevalonate Pathway Prevents Adipocyte Browning in Mice and Men by Affecting Protein Prenylation. *Cell Metab* **29**, 901–916.e8.
- Beaudoin-Bussi eres, G., Laumaea, A., Anand, S.P., Pr evost, J., Gasser, R., Goyette, G., Medjahed, H., Perreault, J., Tremblay, T., Lewin, A., et al. (2020). Decline of humoral responses against SARS-CoV-2 spike in convalescent individuals. *MBio* **11**, e02590-20.
- Brouwer, P.J.M., Caniels, T.G., van der Straten, K., Snitselaar, J.L., Aldon, Y., Bangaru, S., Torres, J.L., Okba, N.M.A., Claireaux, M., Kerster, G., et al. (2020). Potent neutralizing antibodies from COVID-19 patients define multiple targets of vulnerability. *Science* **369**, 643–650.
- Brown, E.P., Licht, A.F., Dugast, A.S., Choi, I., Bailey-Kellogg, C., Alter, G., and Ackerman, M.E. (2012). High-throughput, multiplexed IgG subclassing of antigen-specific antibodies from clinical samples. *J. Immunol. Methods* **386**, 117–123.
- Callow, K.A., Parry, H.F., Sergeant, M., and Tyrrell, D.A. (1990). The time course of the immune response to experimental coronavirus infection of man. *Epidemiol. Infect.* **105**, 435–446.
- Crawford, K.H.D., Eguia, R., Dings, A.S., Loes, A.N., Malone, K.D., Wolf, C.R., Chu, H.Y., Tortorici, M.A., Veessler, D., Murphy, M., et al. (2020). Protocol and Reagents for Pseudotyping Lentiviral Particles with SARS-CoV-2 Spike Protein for Neutralization Assays. *Viruses* **12**, 513.
- Cyster, J.G., and Allen, C.D.C. (2019). B Cell Responses: Cell Interaction Dynamics and Decisions. *Cell* **177**, 524–540.
- Edridge, A.W.D., Kaczorowska, J., Hoste, A.C.R., Bakker, M., Klein, M., Loens, K., Jebbink, M.F., Matser, A., Kinsella, C.M., Rueda, P., et al. (2020). Seasonal coronavirus protective immunity is short-lasting. *Nat. Med.* <https://doi.org/10.1038/s41591-020-1083-1>.
- Grandjean, L., Saso, A., Ortiz, A., Lam, T., Hatcher, J., Thistlewaite, R., Haris, M., Best, T., Johnson, M., Wagstaffe, H., et al. (2020). Humoral Response Dynamics Following Infection with SARS-CoV-2. *medRxiv*. <https://doi.org/10.1101/2020.07.16.20155663>.
- Hagan, T., Cortese, M., Roupheal, N., Boudreau, C., Linde, C., Maddur, M.S., Das, J., Wang, H., Guthmiller, J., Zheng, N.Y., et al. (2019). Antibiotics-Driven Gut Microbiome Perturbation Alters Immunity to Vaccines in Humans. *Cell* **178**, 1313–1328.e13.
- Harritshoej, L., Gybel-Brask, M., Afzal, S., Kamstrup, P., Joergensen, C., Thomsen, M., Hilsted, L., Friis-Hansen, L., Szecsi, P., Pedersen, L., et al. (2020). Comparison of sixteen serological SARS-CoV-2 immunoassays in

sixteen clinical laboratories. medRxiv. <https://doi.org/10.1101/2020.07.30.20165373>.

Hoffmann, M., Kleine-Weber, H., Schroeder, S., Kruger, N., Herrler, T., Erichsen, S., Schiergens, T.S., Herrler, G., Wu, N.H., Nitsche, A., et al. (2020). SARS-CoV-2 Cell Entry Depends on ACE2 and TMPRSS2 and Is Blocked by a Clinically Proven Protease Inhibitor. *Cell* *181*, 271–280.e8.

Hou, H., Wang, T., Zhang, B., Luo, Y., Mao, L., Wang, F., Wu, S., and Sun, Z. (2020). Detection of IgM and IgG antibodies in patients with coronavirus disease 2019. *Clin. Transl. Immunology* *9*, e01136.

Isho, B., Abe, K.T., Zuo, M., Jamal, A.J., Rathod, B., Wang, J.H., Li, Z., Chao, G., Rojas, O.L., Bang, Y.M., et al. (2020). Persistence of serum and saliva antibody responses to SARS-CoV-2 spike antigens in COVID-19 patients. *Sci. Immunol.* *5*, eabe5511.

Iyer, A.S., Jones, F.K., Nodoushani, A., Kelly, M., Becker, M., Slater, D., Mills, R., Teng, E., Kamruzzaman, M., Garcia-Beltran, W.F., et al. (2020). Persistence and decay of human antibody responses to the receptor binding domain of SARS-CoV-2 spike protein in COVID-19 patients. *Sci. Immunol.* *5*, eabe0367.

Ju, B., Zhang, Q., Ge, J., Wang, R., Sun, J., Ge, X., Yu, J., Shan, S., Zhou, B., Song, S., et al. (2020). Human neutralizing antibodies elicited by SARS-CoV-2 infection. *Nature* *584*, 115–119.

Kaneko, N., Kuo, H.H., Boucau, J., Farmer, J.R., Allard-Chamard, H., Mahajan, V.S., Piechocka-Trocha, A., Lefteri, K., Osborn, M., Bals, J., et al. (2020). Loss of Bcl-6-Expressing T Follicular Helper Cells and Germinal Centers in COVID-19. *Cell*. <https://doi.org/10.2139/ssrn.3652322>.

Kiyuka, P.K., Agoti, C.N., Muniyoki, P.K., Njeru, R., Bett, A., Otieno, J.R., Otieno, G.P., Kamau, E., Clark, T.G., van der Hoek, L., et al. (2018). Human Coronavirus NL63 Molecular Epidemiology and Evolutionary Patterns in Rural Coastal Kenya. *J. Infect. Dis.* *217*, 1728–1739.

Long, Q.X., Liu, B.Z., Deng, H.J., Wu, G.C., Deng, K., Chen, Y.K., Liao, P., Qiu, J.F., Lin, Y., Cai, X.F., et al. (2020a). Antibody responses to SARS-CoV-2 in patients with COVID-19. *Nat. Med.* *26*, 845–848.

Long, Q.X., Tang, X.J., Shi, Q.L., Li, Q., Deng, H.J., Yuan, J., Hu, J.L., Xu, W., Zhang, Y., Lv, F.J., et al. (2020b). Clinical and immunological assessment of asymptomatic SARS-CoV-2 infections. *Nat. Med.* *26*, 1200–1204.

Lucas, C., Wong, P., Klein, J., Castro, T.B.R., Silva, J., Sundaram, M., Ellingson, M.K., Mao, T., Oh, J.E., Israelow, B., et al. (2020). Longitudinal analyses reveal immunological misfiring in severe COVID-19. *Nature* *584*, 463–469.

Ma, H., Zeng, W., He, H., Zhao, D., Jiang, D., Zhou, P., Cheng, L., Li, Y., Ma, X., and Jin, T. (2020). Serum IgA, IgM, and IgG responses in COVID-19. *Cell. Mol. Immunol.* *17*, 773–775.

Mathew, D., Giles, J.R., Baxter, A.E., Oldridge, D.A., Greenplate, A.R., Wu, J.E., Alanio, C., Kuri-Cervantes, L., Pampena, M.B., D'Andrea, K., et al.; UPenn COVID Processing Unit (2020). Deep immune profiling of COVID-19 patients reveals distinct immunotypes with therapeutic implications. *Science* *369*, eabc8511.

Mesin, L., Ersching, J., and Victora, G.D. (2016). Germinal Center B Cell Dynamics. *Immunity* *45*, 471–482.

Meyer, B., Torriani, G., Yerly, S., Mazza, L., Calame, A., Arm-Vernez, I., Zimmer, G., Agoritsas, T., Stirnemann, J., Spechbach, H., et al.; Geneva Center for Emerging Viral Diseases (2020). Validation of a commercially available SARS-CoV-2 serological immunoassay. *Clin. Microbiol. Infect.* *26*, 1386–1394.

Oran, D.P., and Topol, E.J. (2020). Prevalence of Asymptomatic SARS-CoV-2 Infection: A Narrative Review. *Ann Intern Med.* <https://doi.org/10.7326/M20-3012>.

Piccoli, L., Park, Y.J., Tortorici, M.A., Czudnochowski, N., Walls, A.C., Beltramello, M., Silacci-Fregni, C., Pinto, D., Rosen, L.E., Bowen, J.E., et al. (2020). Mapping Neutralizing and Immunodominant Sites on the SARS-CoV-2 Spike Receptor-Binding Domain by Structure-Guided High-Resolution Serology. *Cell*. <https://doi.org/10.1016/j.cell.2020.09.037>.

Popescu, M., Cabrera-Martinez, B., and Winslow, G.M. (2019). TNF- $\alpha$  Contributes to Lymphoid Tissue Disorganization and Germinal Center B Cell Suppression during Intracellular Bacterial Infection. *J. Immunol.* *203*, 2415–2424.

Premkumar, L., Segovia-Chumbez, B., Jadi, R., Martinez, D.R., Raut, R., Markmann, A., Cornaby, C., Bartelt, L., Weiss, S., Park, Y., et al. (2020). The receptor binding domain of the viral spike protein is an immunodominant and highly specific target of antibodies in SARS-CoV-2 patients. *Sci. Immunol.* *5*, eabc8413.

Rijkers, G., Murk, J.L., Wintermans, B., van Looy, B., van den Berge, M., Veenemans, J., Stohr, J., Reusken, C., van der Pol, P., and Reimerink, J. (2020). Differences in antibody kinetics and functionality between severe and mild SARS-CoV-2 infections. *J. Infect. Dis.* *222*, 1265–1269.

Robbiani, D.F., Gaebler, C., Muecksch, F., Lorenzi, J.C.C., Wang, Z., Cho, A., Agudelo, M., Barnes, C.O., Gazumyan, A., Finkin, S., et al. (2020). Convergent antibody responses to SARS-CoV-2 in convalescent individuals. *Nature* *584*, 437–442.

Rogers, T.F., Zhao, F., Huang, D., Beutler, N., Burns, A., He, W.T., Limbo, O., Smith, C., Song, G., Woehl, J., et al. (2020). Isolation of potent SARS-CoV-2 neutralizing antibodies and protection from disease in a small animal model. *Science* *369*, 956–963.

Ryg-Cornejo, V., Ioannidis, L.J., Ly, A., Chiu, C.Y., Teller, J., Hill, D.L., Preston, S.P., Pellegrini, M., Yu, D., Nutt, S.L., et al. (2016). Severe Malaria Infections Impair Germinal Center Responses by Inhibiting T Follicular Helper Cell Differentiation. *Cell Rep.* *14*, 68–81.

Seow, J., Graham, C., Merrick, B., Acors, K., Steel, J., Hemmings, O., O'Bryne, A., Kouphou, N., Pickering, S., Galao, R., et al. (2020). Longitudinal evaluation and decline of antibody responses in SARS-CoV-2 infection. medRxiv. <https://doi.org/10.1101/2020.07.09.20148429>.

Takahashi, Y., Dutta, P.R., Cerasoli, D.M., and Kelsoe, G. (1998). In situ studies of the primary immune response to (4-hydroxy-3-nitrophenyl)acetyl. V. Affinity maturation develops in two stages of clonal selection. *J. Exp. Med.* *187*, 885–895.

Takemori, T., Kaji, T., Takahashi, Y., Shimoda, M., and Rajewsky, K. (2014). Generation of memory B cells inside and outside germinal centers. *Eur. J. Immunol.* *44*, 1258–1264.

Tiller, T., Meffre, E., Yurasov, S., Tsuiji, M., Nussenzweig, M.C., and Wardemann, H. (2008). Efficient generation of monoclonal antibodies from single human B cells by single cell RT-PCR and expression vector cloning. *J. Immunol. Methods* *329*, 112–124.

Wang, P., Liu, L., Nair, M.S., Yin, M.T., Luo, Y., Wang, Q., Yuan, T., Mori, K., Solis, A.G., Yamashita, M., et al. (2020). SARS-CoV-2 neutralizing antibody responses are more robust in patients with severe disease. *Emerg. Microbes Infect.* *9*, 2091–2093.

Weisel, F., and Shlomchik, M. (2017). Memory B Cells of Mice and Humans. *Annu. Rev. Immunol.* *35*, 255–284.

Woodruff, M.C., Ramonell, R.P., Nguyen, D.C., Cashman, K.S., Saini, A.S., Haddad, N.S., Ley, A.M., Kyu, S., Howell, J.C., Ozturk, T., et al. (2020). Extra-follicular B cell responses correlate with neutralizing antibodies and morbidity in COVID-19. *Nat Immunol.* <https://doi.org/10.1038/s41590-020-00814-z>.

Wu, Z., and McGoogan, J.M. (2020). Characteristics of and Important Lessons From the Coronavirus Disease 2019 (COVID-19) Outbreak in China: Summary of a Report of 72314 Cases From the Chinese Center for Disease Control and Prevention. *JAMA* *323*, 1239–1242.

Zhou, P., Yang, X.L., Wang, X.G., Hu, B., Zhang, L., Zhang, W., Si, H.R., Zhu, Y., Li, B., Huang, C.L., et al. (2020). A pneumonia outbreak associated with a new coronavirus of probable bat origin. *Nature* *579*, 270–273.

Zhu, N., Zhang, D., Wang, W., Li, X., Yang, B., Song, J., Zhao, X., Huang, B., Shi, W., Lu, R., et al.; China Novel Coronavirus Investigating and Research Team (2020). A Novel Coronavirus from Patients with Pneumonia in China, 2019. *N. Engl. J. Med.* *382*, 727–733.

Zou, H., and Haste, T. (2005). Regularization and variable selection via the elastic net. *J. R. Stat. Soc. B* *67*, 301–320.

STAR★METHODS

KEY RESOURCES TABLE

REAGENT or RESOURCE	SOURCE	IDENTIFIER
<b>Antibodies</b>		
Mouse anti-human IgG1-Fc PE	Southern Biotech	Cat# 9054-09; RRID:AB_2796628
Mouse anti-human IgG2-Fc PE	Southern Biotech	Cat# 9060-09; RRID:AB_2796635
Mouse anti-human IgG3-hinge PE	Southern Biotech	Cat# 9210-09; RRID:AB_2796701
Mouse anti-human IgG4-Fc PE	Southern Biotech	Cat# 9200-09; RRID:AB_2796693
Mouse anti-human IgA1-Fc PE	Southern Biotech	Cat# 9130-09; RRID:AB_2796656
Mouse anti-human IgM-Fc PE	Southern Biotech	Cat# 9020-09; RRID:AB_2796577
Goat anti-human IgG-alkaline phosphatase (AP)	Southern Biotech	Cat# 2040-04; RRID:AB_2795643
Goat anti-human IgM-AP	Southern Biotech	Cat# 2020-04; RRID:AB_2795602
anti-RBD human IgG	Obtained from the lab of Dr. Aaron Schmidt	CR3022; RRID:AB_2848080
Anti-flag-APC	BioLegend	Cat# 637307; RRID:AB_2561496
Anti-flag-PE	BioLegend	Cat# 637310; RRID:AB_2563148
Anti-human-IgG-PerCP-Cy5.5	BioLegend	Cat# 410710; RRID:AB_2565788
Anti-human-CD138-PE-Cy7	BioLegend	Cat# 356514; RRID:AB_2562658
Anti-human-CD27-APC-Cy7	BioLegend	Cat# 356424; RRID:AB_2566773
Anti-human-CD19-BV510	BioLegend	Cat# 302242; RRID:AB_2561668
Anti-human-IgD-AF700	BioLegend	Cat# 348230; RRID:AB_2563335
Anti-human-IgM-BV605	BioLegend	Cat# 314524; RRID:AB_2562374
Anti-human CD27-FITC	BioLegend	Cat# 356404; RRID:AB_2561788
Anti-human CCR7-PE	BioLegend	Cat# 353204; RRID:AB_10913813
Anti-human CD4- PerCP-Cy5.5	BioLegend	Cat# 357414; RRID:AB_2565666
Anti-human CD8-PE-Cy7	BioLegend	Cat# 344712; RRID:AB_2044008
Anti-human CD95-APC	BioLegend	Cat# 305612; RRID:AB_314550
Anti-human CD45RA-APC-Cy7	BioLegend	Cat# 304128; RRID:AB_10708880
Anti-human CD3-AF700	BioLegend	Cat# 300424; RRID:AB_493741
Anti-human CD38-BV711	BioLegend	Cat# 303528; RRID:AB_2563811
Anti-human PD-1-PE-Cy7	BioLegend	Cat# 329918; RRID:AB_2159324
Anti-human CXCR5-APC	BioLegend	Cat# 356908; RRID:AB_2561817
Anti-human CD8-BV510	BioLegend	Cat# 344732; RRID:AB_2564624
Anti-human ICOS-BV605	BioLegend	Cat# 313538; RRID:AB_2687079
<b>Biological Samples</b>		
COVID-19 convalescent plasma	This manuscript	N/A
pre-COVID19 plasma (collected before 10/01/2019)	This manuscript	N/A
<b>Chemicals, Peptides, and Recombinant Proteins</b>		
SARS-CoV-2 S (Luminex)	Obtained from the lab of Dr. Eric Fischer	N/A
SARS-CoV-2 RBD	Obtained from the lab of Dr. Aaron Schmidt	N/A
SARS-CoV-2 S1	Sino Biological	CAT # 40591-V08H
SARS-CoV-2 S2	Sino Biological	CAT # 40590-V08B
OC43 RBD	Obtained from the lab of Dr. Aaron Schmidt	N/A
NL63 RBD	Obtained from the lab of Dr. Aaron Schmidt	N/A
229E RBD	Obtained from the lab of Dr. Aaron Schmidt	N/A
NL63 RBD	Obtained from the lab of Dr. Aaron Schmidt	N/A
SARS-CoV-2 N (Luminex)	Aalto Bio Reagents	CAT # CK 6404-b

(Continued on next page)

**Continued**

REAGENT or RESOURCE	SOURCE	IDENTIFIER
SARS-CoV-2 NTD	Kindly provided by Moderna, Inc.	N/A
Human Fc receptors	Produced at the Duke Human Vaccine Institute	N/A
Streptavidin-R-phycoerythrin	Prozyme	Cat# PJ31S
SARS-CoV-2 nucleocapsid protein (ELISA)	GenScript	Cat# Z03480
Spike protein (ELISA)	Obtained from the lab of Bing Chen	N/A
Sodium carbonate	Fisher Scientific	Cat# S263
Sodium bicarbonate	Fisher Scientific	Cat# S233
Bovine serum albumin (BSA)	Sigma	Cat# A2153
Triton X-100	Fisher Scientific	Cat# 9002-93-1
10x phosphate buffered saline (PBS)	Boston BioProducts	Cat# BM-220-10XS
Glycine	Sigma-Aldrich	Cat# G7126
Zinc chloride	Sigma-Aldrich	Cat# 793523
Magnesium chloride	Sigma-Aldrich	Cat# M0250
Tween-20	Sigma-Aldrich	Cat# P1379
Ficoll-Paque PLUS	Cytiva	Cat# 17144003
Anti-human CD19 magnetic microbeads	Miltenyi	Cat# 130-050-301
Spike protein with His and Flag tags	GenScript	Cat# Z03481
4',6-diamidino-2-phenylindole, dihydrochloride (DAPI)	Thermo Fisher Scientific	Cat# D1306
Dithiothreitol (DTT)	Thermo Fisher Scientific	Cat# R0861
RNaseOUT	Thermo Fisher Scientific	Cat# 10777-019
Random hexamer primer	Thermo Fisher Scientific	Cat# FERSO142
10 mM dNTPs	Promega	Cat# U1515
IGEPAL CA-630	Sigma-Aldrich	Cat# I8896
SuperScript III reverse transcriptase	Thermo Fisher Scientific	Cat# 18080085
HotStarTaq DNA polymerase	QIAGEN	Cat# 203205
Lipofectamine 3000 transfection reagent	Thermo Fisher Scientific	Cat# L3000008
<b>Deposited Data</b>		
Primary data	This paper	Mendeley Data <a href="https://doi.org/10.17632/3dxv7mzb76.1">https://doi.org/10.17632/3dxv7mzb76.1</a>
<b>Critical Commercial Assays</b>		
BirA-500: BirA biotin-protein ligase standard reaction kit	Avidity	Cat#: BirA500
SARS-CoV-2 Surrogate Virus Neutralization Test (sVNT) Kit	GenScript	Cat# L00847
ONE-Glo luciferase assay system	Promega	Cat# E6120
<b>Experimental Models: Cell Lines</b>		
HEK293T	ATCC	Cat# CRL-3216
293T/17	ATCC	Cat# CRL-11268
ACE2/TMPRSS2-expressing HEK293T	Obtained from the lab of Marc Johnson	N/A
ACE2-expressing HEK293T	Obtained from the lab of Michael Farzan	N/A
<b>Oligonucleotides</b>		
Primer set for Ig PCR (see <a href="#">Tiller et al., 2008</a> )	IDT DNA	N/A
<b>Recombinant DNA</b>		
HDM-SARS2-Spike-delta21	Addgene	Cat#155130
pLenti CMV Puro LUC (w168-1)	Addgene	Cat#17477
psPAX2	Addgene	Cat#12260

(Continued on next page)

**Continued**

REAGENT or RESOURCE	SOURCE	IDENTIFIER
Software and Algorithms		
GraphPad Prism V8.2.1	GraphPad Software	<a href="https://www.graphpad.com/scientific-software/prism/">https://www.graphpad.com/scientific-software/prism/</a>
Intellicyt ForeCyt Software	Sartorius	<a href="https://intellicyt.com/products/software/">https://intellicyt.com/products/software/</a>
IgBLASTn v. 1.16.0	NCBI	<a href="ftp://ftp.ncbi.nih.gov/blast/executables/igblast/release/LATEST">ftp://ftp.ncbi.nih.gov/blast/executables/igblast/release/LATEST</a>
Intellicyt ForeCyt Software	Sartorius	<a href="https://intellicyt.com/products/software/">https://intellicyt.com/products/software/</a>
R	Free Software Foundation/GNU	R v4.0.0
Bioconductor software in R	Bioconductor	<a href="https://www.bioconductor.org/">https://www.bioconductor.org/</a>
Python	Python Software Foundation	Python v3.7.0
Python using the scikit-learn package	Python Software Foundation	<a href="https://pypi.org/project/scikit-learn/">https://pypi.org/project/scikit-learn/</a>
Cytoscape	NIGMS	Cytoscape v3.8.0
Other		
MagPlex microspheres	Luminex corporation	CAT#: MC12001-01, MCI12040-01, MCI10077-01

**RESOURCE AVAILABILITY****Lead Contact**

Further information and requests for resources and reagents should be directed to and will be fulfilled by the Lead Contact, Duane R. Wesemann. [dwesemann@bwh.harvard.edu](mailto:dwesemann@bwh.harvard.edu).

**Materials Availability**

No unique materials were generated for this study.

**Data and Code Availability**

All primary data reported in this study are available at Mendeley Data (<https://doi.org/10.17632/3dxv7mzb76.1>).

**EXPERIMENTAL MODEL AND SUBJECT DETAILS****Human study participants**

This study and protocol were approved by the Partners Institutional Review Board. Participants were recruited through advertisements including flyers posted in Boston area hospitals and online through an institutional website for clinical studies open to the public. 26 male and 66 female volunteers aged 18 and older with a history of COVID-19 were enrolled between March and June 2020. COVID-19 was diagnosed by a healthcare professional based on symptoms and a positive nasopharyngeal swab RT-PCR test. Positive RT-PCR tests were verified by study staff. After enrollment, the clinical team determined one subject was diagnosed not by PCR test but by Quest Diagnostics antibody test and symptomatology consistent with COVID-19. Blood samples were obtained from March 2020-June 2020 via antecubital venipuncture. Participants completed questionnaires regarding demographic information, medical history, and risk factors for SARS-CoV-2 exposure. Participants self-reported any personal history of lung disease, cardiovascular disease, diabetes, immunocompromise (either due to a medical condition or medication use) and symptoms and characteristics of their COVID-19 clinical course. Participants rated the severity of their COVID-19 symptoms on a 1-10 scale, with 1 describing very mild symptoms and 10 describing very severe symptoms. Participants self-reported the symptom onset date, and the symptom recovery date. Of the 92 participants who donated a first blood sample, 5 participants with a long-term mild symptom component donated their first blood sample before their reported final symptom resolution date. All others were collected following completion of full symptom resolution. Symptom duration is calculated by subtracting the symptom recovery date and the symptom onset date. Detailed demographic and other information describing the cohort are provided in [Table S1](#). BMI indicates body mass index. It was calculated by the participant's weight in kilograms divided by the square of their height in meters.

## METHOD DETAILS

### ELISA

96-well polystyrene plates (Thermo Fisher) were coated with 30  $\mu\text{L}$  of 0.6  $\mu\text{g}/\text{mL}$  N protein (Genscript), 0.3  $\mu\text{g}/\text{mL}$  S (gift of Bing Chen, Ragon Institute of MGH, MIT and Harvard) or 0.6  $\mu\text{g}/\text{mL}$  RBD (gift of Aaron Schmidt, Ragon Institute of MGH, MIT and Harvard) diluted in bicarbonate buffer (0.1M) and incubated overnight at 4°C. Coat solutions were discarded and 100  $\mu\text{L}$  of 3% BSA in PBS added to each well to block. Blocking was performed for > 2 h at room temperature. During the block step, plasma was thawed at room temperature, combined with an equal volume of 2% Triton in PBS (Thermo Fisher) and incubated for 20 min at room temperature to inactivate enveloped viruses. Dilutions of plasma and standards were made using 1% BSA and 0.05% Tween-20 in PBS as diluent. Block solution was discarded and plates washed with 0.05% Tween-20 in PBS. Plasma dilutions were then applied to the plates and they were placed at 4°C overnight. Following the plasma incubation step, plates were washed three times with 0.05% Tween-20 in PBS. Secondary antibody solutions of anti-human IgG-alkaline phosphatase (AP) diluted 1:2000 in 1% BSA and 0.05% Tween-20 or anti-human IgM-AP at a 1:1000 dilution in 1% BSA and 0.05% Tween-20 (Southern Biotech, Birmingham, AL) were prepared and 30  $\mu\text{L}$  distributed to each well. Secondary antibodies were incubated on the plates for 90 min at room temperature and then three washes performed. Alkaline phosphatase substrate p-nitrophenyl phosphate tablets (Sigma, St. Louis, MO) were dissolved in 0.1 M glycine, pH 10.4, with 1 mM  $\text{MgCl}_2$  and 1 mM  $\text{ZnCl}_2$ , pH 10.4 to a concentration of 1.6 mg/mL and 100  $\mu\text{L}$  of this development solution distributed to each well. Plates were placed in the dark and allowed to develop for 2 h prior to reading. Absorbance at 405 nm was measured using a microplate reader (Biotek Synergy H1). All samples were run in duplicate wells.

For quantitation of plasma IgG or IgM reactive to SARS-CoV-2 antigens, a 2x dilution series was produced from an initial 100x plasma dilution for each sample. A 2x dilution series of either a pooled COVID-19 convalescent plasma or RBD-binding monoclonal IgG1, CR3022, were included on each plate as controls. A standard curve was produced by non-linear regression with Graphpad software from the control values. The Ig level for each unknown sample was determined by interpolation for a single dilution with an  $\text{OD}_{405,405\text{nm}}$  falling in the mid-range of the standards. Where a polyclonal standard was used, antibody levels are reported in reference to the standard as arbitrary units (AU). Where CR3022 was used a standard, antibody levels are reported as CR3022 concentration equivalents (mAb  $\mu\text{g}/\text{mL}$  equivalents).

Pre-COVID19 plasma from four healthy subjects were included as negative controls on each ELISA plate. These pre-COVID19 plasma were collected before 10/01/2019.

### Luminex assay

A custom multiplexed Luminex assay was used to measure relative titer of antigen-specific subclasses, isotypes and Fc-receptors (FcRs), as previously described (Brown et al., 2012). Briefly, antigen was covalently coupled to carboxyl-beads using EDC (Thermo Fisher) and Sulfo-NHS (Thermo Fisher). Antigen used in the Luminex assay include SARS-CoV-2 RBD, OC43 RBD, NL63 RBD, 229E RBD, NL63 RBD (all kindly provided by Aaron Schmidt, Ragon Institute), SARS-CoV-2 N protein (Aalto Bio Reagents), SARS-CoV-2 N-terminal domain (NTD) (kindly provided by Moderna, Inc.) and SARS-CoV-2 S (kindly provided by Eric Fischer, Dana Farber) as well as S1 (Sino Biological) and S2 (Sino Biological) subunits of S. Antigen-coupled beads were blocked, washed with PBS-Tween, re-suspended in PBS and stored at 4°C. Plasma was diluted (1:500 for IgG1, 1:1000 for all Fc- receptors, and 1:100 for all other isotype/subclass readouts). Immune complexes were formed by overnight incubation of diluted plasma and antigen-coupled beads at 4°C, shaking at 700 rpm. The following day, plates were washed with an automated plate washer (Tecan) with 0.1% BSA 0.02% Tween-20. Antigen-specific antibody titers were detected with PE-coupled secondaries (Southern Biotech). For FcR-binding, FcRs with an AviTag (Duke Protein Production Facility) were biotinylated with BirA500 kit (Avidity). For detection of FcR binding, FcRs were labeled with PE before addition to the immune complex. Fluorescence was detected using an Intellicyt iQue and analyzed using Forecyt software.

### Multi-variate analysis of symptom severity

Prior to multi-variate analysis, each Luminex and ELISA-derived feature was box-cox transformed, centered and scaled to unit variance. OPLS-DA was performed on a feature set reduced via elastic net regularization and variable selection. Elastic net minimizes the number of features needed in the model without forfeiting model performance (Zou and Hastie, 2005). All ElasticNet parameters were optimized using a `tuneLength = 10` and leave-one-out cross validation. The final reduced feature set included variables selected in 80% or more of 100 rounds of the elastic net algorithm. The R 'ropls' package was used to implement OPLS-DA (`orth1 = 1`; `Pred1 = 1`). An AUC-ROC curve was generated to evaluate the performance of the model using the python 'sklearn.metrics' package. Pairwise spearman's correlation tests were performed comparing each feature in the dataset to the four features included in the final OPLS-DA model. Correlations with coefficients greater than 0.75 and  $p < 0.1$  were inputted into Cytoscape to generate correlation networks. To divide symptoms scores into low and high, we chose 1-4 for low, and 5-10 for high due to the fact that the distribution was bimodal with one peak at 3 and the other at 5, so 4 is a natural dividing point.

### FACS sorting and monoclonal antibody sequence isolation from memory B cells

PBMCs were isolated by FicolI (GE Lifesciences) separation from blood. B cells were enriched from total PBMCs using anti-CD19-conjugated magnetic beads (Miltenyi). Flow-through cells were used to analyze T cell populations. Following enrichment, B cells were incubated with 2  $\mu\text{g}/\text{mL}$  flag-tagged S protein (Genscript) on ice for 30 min. Cells were then washed and incubated with both APC and PE conjugated anti-Flag antibodies to double stain S-binding B cells. Surface-marker targeting stains were simultaneously applied with the anti-flag antibodies. DAPI<sup>-</sup>IgM<sup>-</sup>IgD<sup>-</sup>IgG<sup>+</sup>CD27<sup>+</sup>Spike<sup>+</sup> cells were single sorted in 96 well plates containing 4  $\mu\text{L}/\text{well}$  of ice-cold lysis buffer (0.5x PBS containing 10mM DTT, and 4 U RNaseout). Plates were sealed with AlumaSeal 96 film (Sigma), and immediately frozen on dry ice before transfer to a  $-80^{\circ}\text{C}$  freezer. The RT-PCR and sequencing of Ig transcripts was performed as described (Tiller et al., 2008). Briefly, single cell RNA was reverse transcribed with 200 ng random hexamer primer (Thermo Fisher), 1  $\mu\text{L}$  10mM of dNTP (Promega), 0.7  $\mu\text{L}$  100 mM DTT, 0.1  $\mu\text{L}$  RNaseout, 0.5% v/v Igepal CA-630 (Sigma), and 50 U superscript III reverse transcriptase (Thermo Fisher). The reverse transcription reaction was performed in a thermocycler using the following program:  $42^{\circ}\text{C}$  for 10 min,  $25^{\circ}\text{C}$  for 10min, and  $50^{\circ}\text{C}$  for 60 min. Subsequently, 2  $\mu\text{L}$  of cDNA was used to amplified Ig sequences by separate heavy,  $\kappa$  light chain and  $\lambda$  light chain-targeting nested PCRs. Each reaction was performed in a 20  $\mu\text{L}$  volume containing 250 nM primer mix, 250 nM dNTP mix (Promega) and 0.5 U HotStar Taq DNA polymerase (QIAGEN). Two rounds of amplification were performed for 35 cycles at  $94^{\circ}\text{C}$  for 30 s,  $58^{\circ}\text{C}$  (IgH/Ig $\kappa$ ) or  $60^{\circ}\text{C}$  (Ig $\lambda$ ) for 30 s,  $72^{\circ}\text{C}$  for 55 s (1st PCR) or 45 s (2nd PCR). The PCR products from the second PCR were sent for Sanger sequencing with reverse primers. The sequences were trimmed based on quality score provided by the service provider (GENEWIZ) and aligned by IgBlastn v.1.16.0 with IMGT annotated germline sequences. To determine somatic hypermutations, productive and in-frame IGHV nucleotide sequences were aligned to their closest germline sequences (Robbiani et al., 2020).

### ACE2-binding inhibition assay

Inhibition of RBD binding to ACE2 by plasma was measured using a commercial kit supplied by Genscript as described by the manufacturer. In brief, RBD conjugated to HRP was incubated with dilutions of plasma from 1:5, 1:10, 1:30, 1:90, 1:270, to 1:810 in supplied dilution buffer for 30 min at  $37^{\circ}\text{C}$ . 100  $\mu\text{L}$  of plasma and RBD-HRP solutions were then applied to a microtiter plate coated with recombinant ACE2 and incubated at  $37^{\circ}\text{C}$  for 1 h. The plates were then washed 4 times with the supplied wash solution and 100  $\mu\text{L}$  of TMB applied to each well. Plates were then incubated in the dark at  $25^{\circ}\text{C}$  for 15 min and development quenched using 50  $\mu\text{L}$  of stop solution. Absorbance at 450 nm was then read using a microplate reader (Biotek Synergy H1). Positive and negative controls were provided with the kit. Percent of inhibition was calculated by  $(1 - \text{OD value of sample/average OD value of negative controls}) \times 100\%$ . Non-linear regression was performed using Graphpad Prism software to determine the 50% inhibitory concentration ( $\text{IC}_{50}$ ) titer.  $\text{IC}_{50}$  values derived from curves with goodness of fit less than 0.7 or  $\text{IC}_{50}$  values less than 1 in initial and follow up blood draws were excluded from further analysis.

### Conventional SARS-CoV-2 pseudovirus neutralization assay

Neutralizing activity against SARS-CoV-2 pseudovirus was measured using a single-round infection assay in 293T/ACE2/TMPRSS2 target cells. Pseudotyped virus particles were produced in HEK293T cells (ATCC) by co-transfection of three plasmids: pHDM-SARS2-Spike-delta21, pLenti CMV Puro LUC (w168-1), and psPAX2 (Addgene). The HEK293T cell line stably overexpressing the human ACE2 cell surface receptor protein and TMPRSS2 was kindly provided by Dr. Marc Johnson (University of Missouri School of Medicine). For neutralization assays, serial dilutions of patient plasma samples were performed in duplicate followed by addition of pseudovirus. Plates were incubated for 1 h at  $37^{\circ}\text{C}$  followed by addition to target cells ( $2 \times 10^4/\text{well}$ ). Wells containing cells and pseudovirus (without sample) or cells alone acted as positive and negative infection controls, respectively. Assays were harvested on day 2 using Promega One-Glo luciferase reagent and luminescence detected with a Biotek Synergy H1. Titers are reported as the plasma dilution that inhibited 50% of infection ( $\text{NT}_{50}$ ), which was determined by non-linear regression using Graphpad Prism. Samples with  $\text{NT}_{50}$  derived from curves with goodness of fit less than 0.7 were excluded due to technical error unless the lowest dilution (i.e., 1:30) returned values less than 50% neutralization, in which case the  $\text{NT}_{50}$  were included as the detection limit (i.e, 30). Subjects with  $\text{NT}_{50}$  values no more than 30 (the detectable limit) were excluded from durability index calculations.

### High-throughput SARS-CoV-2 pseudovirus neutralization assay

Lentiviral vector-based pseudovirus neutralization assays were performed as previously described (Crawford et al., 2020). Briefly, HEK293T cells were transiently transfected with a combination of pHAGE2-CMV-Luciferase-IRES-ZsGreen-W transfer vector and four separate helper plasmids encoding HIV-GagPol, Rev, Tat and the SARS-CoV-2 spike protein. Pseudovirus was collected and frozen for subsequent neutralization assays. Neutralization assays were performed by mixing the indicated dilution of plasma with pseudovirus for 1 h, prior to the addition of ACE2-expressing 293T target cells (a gift of Michael Farzan). After incubation at  $37^{\circ}\text{C}$  with 5%  $\text{CO}_2$  for 60 h, luciferase signal was measured using a SpectraMAX L instrument. Non-linear regression was performed using Graphpad Prism software to determine  $\text{NT}_{50}$ .  $\text{NT}_{50}$  values derived from curves with goodness of fit less than 0.7 were excluded from further analysis.

### QUANTIFICATION AND STATISTICAL ANALYSIS

GraphPad Prism 8 software was used for all data analyses excluding multivariate analysis, which is described in detail above. Lognormality of antibody titration data was confirmed by Shapiro-Wilk test and Student's t test was used for comparisons of log-transformed antibody levels. Single comparisons between other metrics were performed using Mann-Whitney U test and multiple comparisons were performed using Kruskal-Wallis test. For single variate correlation analyses involving continuous and categorical data, Spearman correlation analysis was performed. Measured p values are presented with relevant datasets or described in the text.

# Supplemental Figures

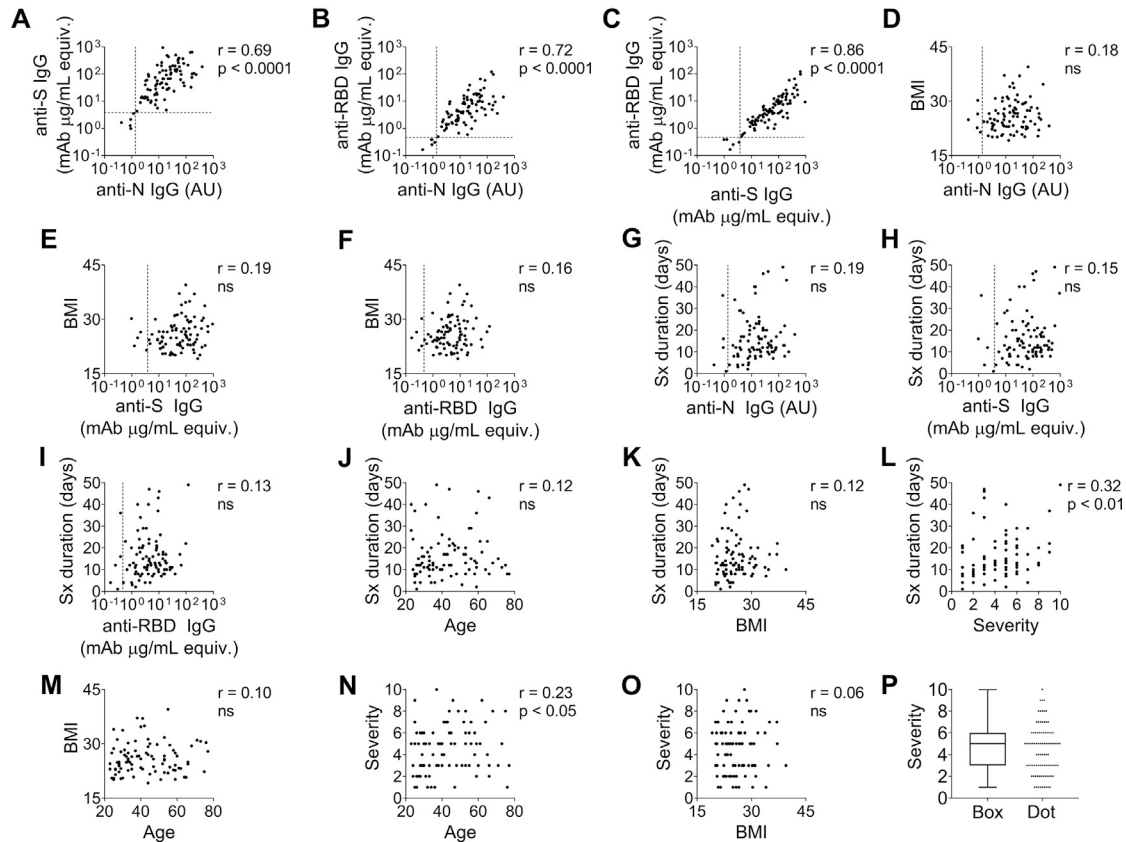


**Figure S1. Correlation Scatterplots for All Baseline Antibody and Clinical Parameters, Related to Figure 1**

Scatterplots illustrating all correlations in Figure 1C. Correlations are shown for (A) anti-N IgG and anti-S IgG levels, (B) anti-N IgG and anti-RBD IgG, (C) anti-S IgG and anti-RBD IgG, (D) anti-N IgG and BMI, (E) anti-S IgG and BMI, (F) anti-RBD IgG and BMI, (G) anti-N IgG and symptom duration, (H) anti-S IgG and symptom duration, (I) anti-RBD IgG and symptom duration, (J) age and symptom duration, (K) BMI and symptom duration, (L) symptom severity and symptom duration, (M) age and BMI, (N) age and symptom severity, (O) and BMI and symptom severity. At the top of each plot is the  $r$  value and significance level determined by Spearman correlation analysis. (P) Box and whisker and dot plots illustrating the range of symptom severity scores reported by subjects.

		Sx			
		Age	BMI	duration	Severity
IgG1	Influenza	r = -0.64 ****	r = 0.04 ns	r = 0.10 ns	r = -0.20 ns
	HKU.1	r = -0.28 *	r = -0.24 ns	r = 0.03 ns	r = -0.09 ns
	229E	r = 0.40 **	r = -0.03 ns	r = 0.06 ns	r = 0.32 *
	OC43	r = 0.10 ns	r = -0.10 ns	r = 0.11 ns	r = 0.19 ns
IgG2	Influenza	r = -0.61 ****	r = 0.08 ns	r = 0.06 ns	r = -0.21 ns
	HKU.1	r = -0.25 ns	r = -0.26 ns	r = 0.08 ns	r = -0.11 ns
	229E	r = 0.22 ns	r = -0.10 ns	r = 0.02 ns	r = 0.21 ns
	OC43	r = 0.16 ns	r = -0.11 ns	r = 0.10 ns	r = 0.11 ns
IgG3	Influenza	r = -0.21 ns	r = -0.03 ns	r = 0.07 ns	r = 0.13 ns
	HKU.1	r = -0.07 ns	r = 0.17 ns	r = 0.08 ns	r = 0.15 ns
	229E	r = 0.11 ns	r = 0.05 ns	r = 0.15 ns	r = 0.28 *
	OC43	r = -0.11 ns	r = 0.01 ns	r = 0.17 ns	r = 0.16 ns
IgG4	Influenza	r = -0.02 ns	r = -0.15 ns	r = -0.06 ns	r = -0.06 ns
	HKU.1	r = -0.05 ns	r = -0.01 ns	r = -0.07 ns	r = 0.07 ns
	229E	r = 0.05 ns	r = 0.08 ns	r = -0.08 ns	r = 0.19 ns
	OC43	r = 0.07 ns	r = 0.09 ns	r = 0.07 ns	r = 0.06 ns
IgA1	Influenza	r = -0.04 ns	r = -0.16 ns	r = 0.14 ns	r = 0.07 ns
	HKU.1	r = -0.25 ns	r = -0.10 ns	r = -0.02 ns	r = -0.01 ns
	229E	r = 0.08 ns	r = 0.17 ns	r = -0.06 ns	r = -0.19 ns
	OC43	r = -0.03 ns	r = -0.02 ns	r = -0.14 ns	r = -0.05 ns
IgM	Influenza	r = -0.28 *	r = -0.07 ns	r = -0.08 ns	r = -0.03 ns
	HKU.1	r = -0.40 **	r = -0.15 ns	r = 0.08 ns	r = -0.08 ns
	229E	r = -0.25 ns	r = -0.21 ns	r = -0.02 ns	r = -0.11 ns
	OC43	r = -0.12 ns	r = -0.23 ns	r = 0.02 ns	r = 0.18 ns

(legend on next page)

---

**Figure S2. Correlations between Influenza or Cold Virus Antibody Levels and Key COVID-19 Cohort Characteristics, Related to Figure 2**  
Heatmap illustrating correlations between IgG1, IgG2, IgG3, IgG4, IgA and IgM reactivity to the spike receptor binding domains of 3 common cold coronaviruses, HKU.1, 229E and OC43, influenza hemagglutinin and key clinical and disease features of subjects in our cohort. Data are from Luminex assay, with 60 subjects included. Survey data are > 96% complete for each category. Spearman correlation analysis was performed and r values and significance levels are displayed, ns is not significant, \*p < 0.05, \*\*p < 0.01, \*\*\*p < 0.001, and \*\*\*\*p < 0.0001. Blue color intensity indicates strength of negative correlations, red color intensity indicates strength of positive correlations.

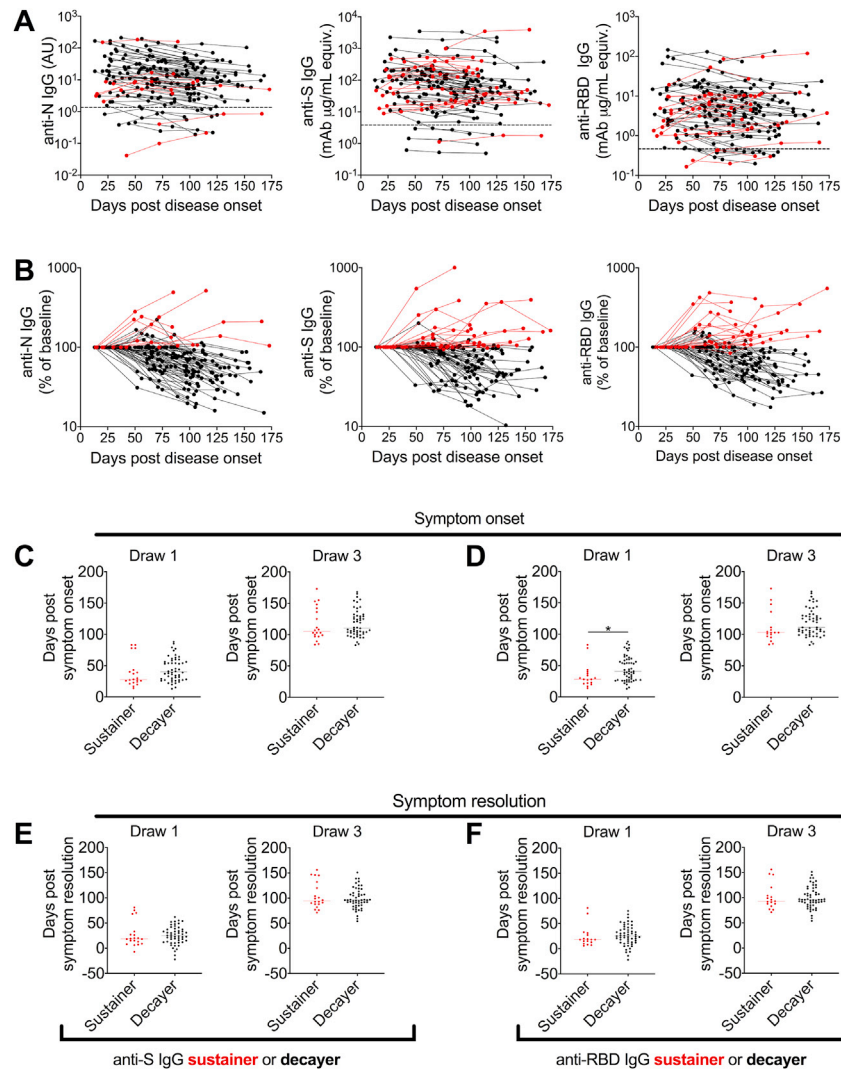
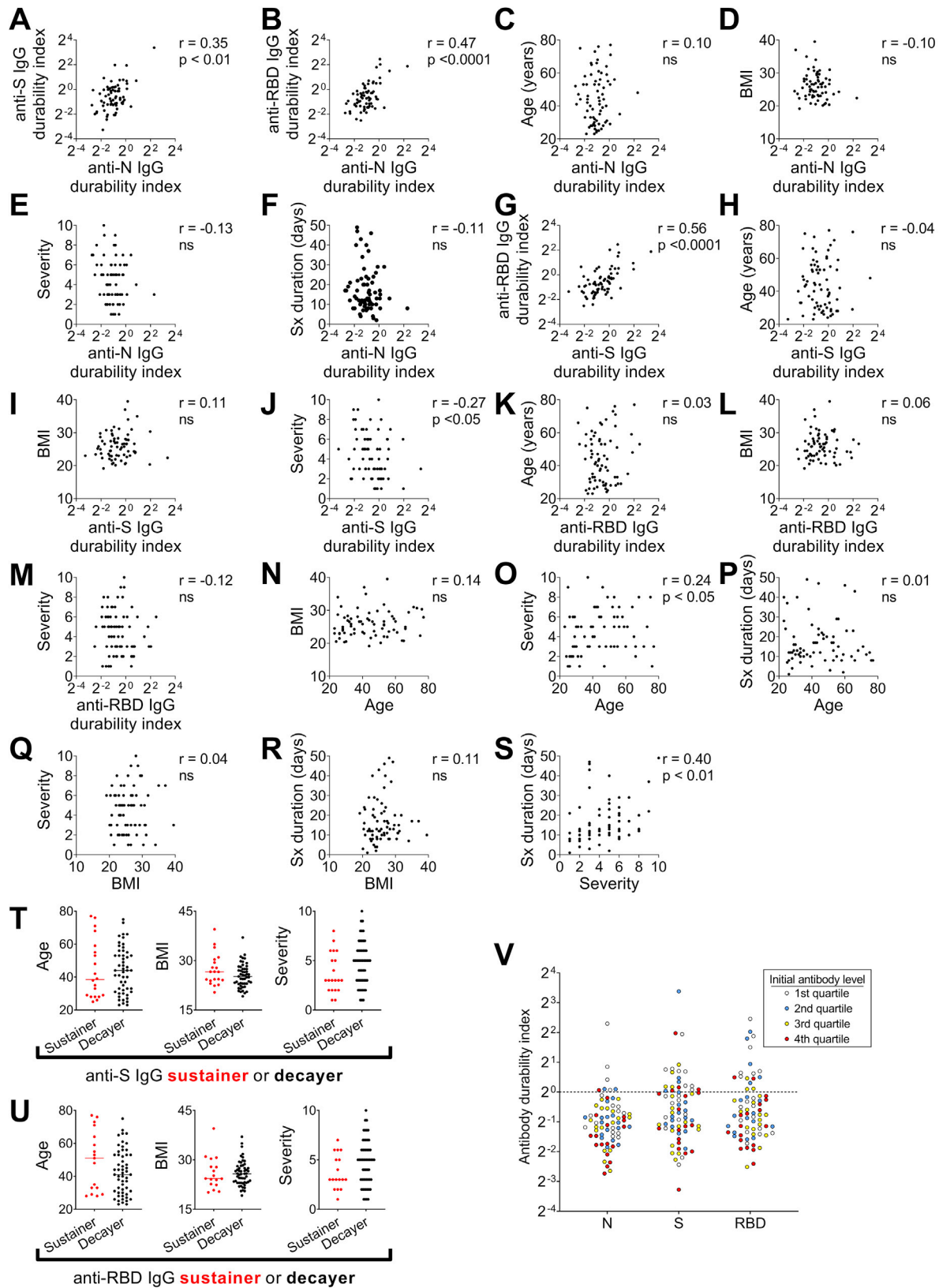


**Figure S3. Alternative Presentation of Anti-SARS-CoV-2 IgG Dynamics over Time and Comparison of Sustainer and Decayer Draw Times, Related to Figure 3**

(A) Scatterplots illustrating changes in anti-N (left), anti-S (middle) and anti-RBD (right) IgG over time in COVID-19 subjects that donated 3 blood samples over approximately 100 days following the onset of their symptoms ( $n = 76$ ). Data for each subject are plotted with sequential draws from an individual linked by connecting lines. Instead of plotting by draw number as in Figure 3 the exact draw time was used. Sustainers are highlighted in red and decayers are displayed in black. The black dashed lines represent twice the average of negative controls as described in Figure 1.

(B) Alternative display of the data in (A), normalizing the anti-SARS-CoV-2 IgG levels of the second and third blood collection as a percent of the value in the first blood samples (baseline) for that subject.

(C–F) Comparison of blood draw time for seroconverted ( $n = 64$ ) anti-S IgG sustainer and decayer (left panels, C and E) and anti-RBD IgG sustainer and decayer (right panels, D and F) relative to symptom onset (top panels, C and D) or relative to symptom resolution (bottom panels, E and F). No significant differences were found in draw times by Mann-Whitney U test except for ((D) draw 1.  $*p < 0.05$ .



(legend on next page)

---

**Figure S4. Correlation Scatterplots for All IgG Durability Indices and Direct Comparison of Clinical Parameters between Sustainers and Decayers, Related to Figure 3**

Scatterplots illustrating all correlations in Figure 3F. Correlations are shown for (A) anti-N and anti-S durability indices, (B) anti-N and anti-RBD durability indices, (C) anti-N durability index and age, (D) anti-N durability index and BMI, (E) anti-N durability index and symptom severity, (F) anti-N durability index and symptom duration, (G) anti-S and anti-RBD durability indices, (H) anti-S durability index and age, (I) anti-S durability index and BMI, (J) anti-S durability index and symptom severity, (K) anti-RBD durability index and age, (L) anti-RBD durability index and BMI, (M) anti-RBD durability index and symptom severity, (N) age and BMI, (O) age and symptom severity, (P) age and symptom duration, (Q) BMI and symptom severity, (R) BMI and symptom duration, and (S) symptom severity and symptom duration. Included at the top of each plot is the  $r$  value and significance level determined by Spearman correlation analysis. (T&U) Comparisons of age (left), BMI (center), and symptom severity (right) between anti-S IgG (T) and anti-RBD IgG (U) sustainers ( $n = 20$ , and  $n = 17$ ) and decayers ( $n = 17$ , and  $n = 55$ ). Sustainers are shown in red and decayers in black. (V) Alternative presentation of Figure 3B, with each point colored to indicate the initial antibody level for that subject. White dots had an initial antibody level falling within the first quartile of measured values (lowest), blue the second quartile, yellow the third quartile, and red the fourth quartile. The dashed line at  $2^\circ$  (i.e., 1) separates sustainers and decayers. In this version,  $n = 72$  as the four subjects negative for SARS-CoV-2 antibody were excluded to maintain consistency with the analysis in Figures 3F–3L. Significance testing for (T) and (U) used the Mann-Whitney U test, no significant differences found.

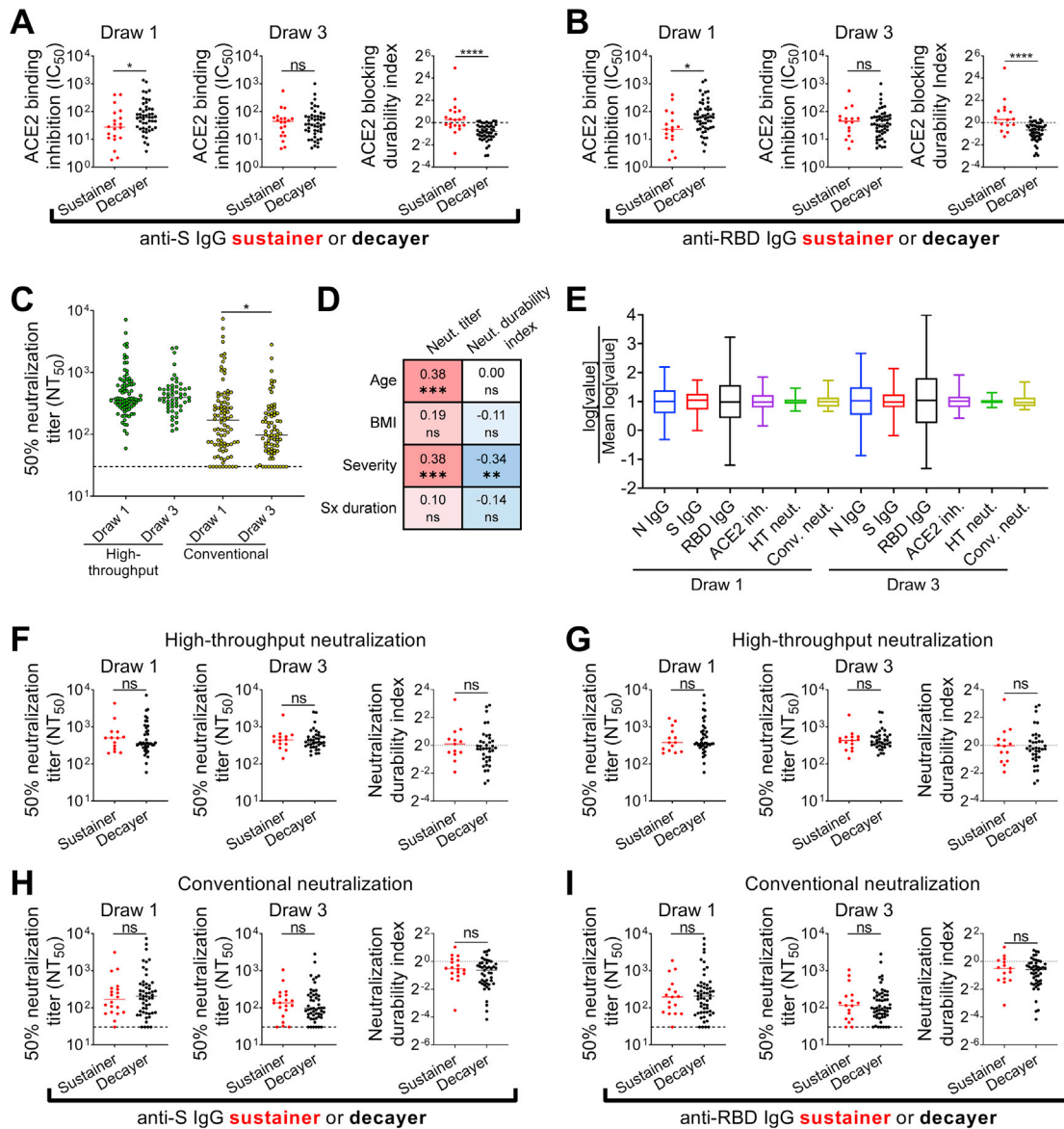


**Figure S5. Comparison of Functional Antibody Data for Sustainers and Decayers, Related to Figure 3**

(A and B) Comparison of ACE2-binding inhibition titers and durability indices of anti-S (A) sustainers (red,  $n = 20$ ) and decayers (black,  $n = 49$ ) as well as anti-RBD (B) sustainers ( $n = 17$ ) and decayers ( $n = 52$ ) described in Figure 3. The ACE2 inhibition durability index was calculated by dividing the 50% inhibitory concentration (IC<sub>50</sub>) titer in draw 3 by the IC<sub>50</sub> titer in draw 1 for subjects with titers exceeding negative controls. The dashed line at 2° (i.e., 1) indicates stable ACE2-inhibition ability across draws 1 and 3.

(C) 50% neutralization titers (NT<sub>50</sub>) at draws 1 and 3 from an automated, high-throughput (green circles, draw 1  $n = 86$  and draw 3  $n = 55$ ) or conventional pseudovirus neutralization assay (gold circles, draw 1  $n = 91$  and draw 3  $n = 76$ ), with the dashed line indicating limit of detection.

(D) Spearman correlation analysis correlating conventional draw 1 NT<sub>50</sub> values (Neut. titer,  $n = 91$ ) or NT<sub>50</sub> durability index (Neut. durability index,  $n = 64$ ) and clinical parameters displayed in a grid. For each correlation, the  $r$  value is given and significance levels are given. Red color intensity indicates strength of positive correlation, intensity of blue indicates strength of negative correlation.

(E) Box and whisker plots illustrating differences in the distributions of values in each antibody measure dataset for the COVID-19 cohort. N IgG, S IgG and RBD IgG are IgG levels as measured by ELISA ( $n = 92$  for draws 1 and 3). ACE2 inh. is the IC<sub>50</sub> titer for ACE2-binding inhibition assay ( $n = 69$  for draw 1,  $n = 68$  for draw 3). HT neut. is NT<sub>50</sub> value as measured by the high-throughput neutralization assay ( $n = 86$  for draw 1,  $n = 55$  for draw 3). Conv. neut. is NT<sub>50</sub> measured by a conventional pseudovirus neutralization assay ( $n = 91$  for draw 1,  $n = 76$  for draw 3). Each value was log transformed and divided by the mean value for that measure. A broader distribution indicates higher variance in the distribution.

(F–I) Analysis of differences in high-throughput neutralization titers (F and G) and conventional neutralization titers (H and I) between anti-S (F and H) and anti-RBD (G and I) sustainers and decayers as described for ACE2 binding inhibition in (A) and (B). Significance testing for all comparisons used the Mann-Whitney U test. Significance is reported in the panels, ns is not significant, \* $p < 0.05$ , \*\* $p < 0.01$ , \*\*\* $p < 0.001$ , and \*\*\*\* $p < 0.0001$ .

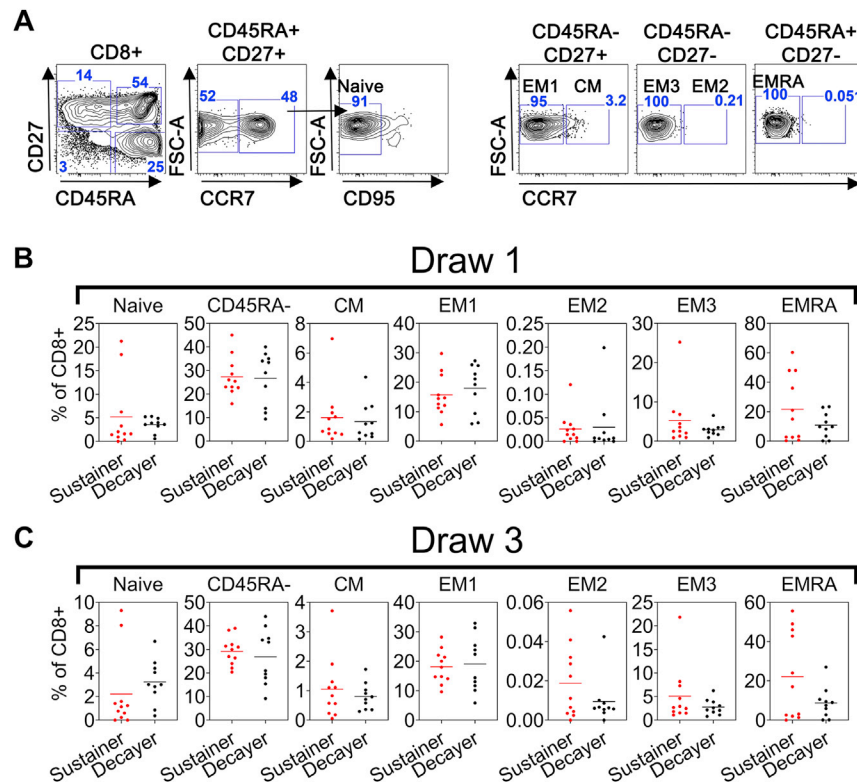


**Figure S6. Comparison CD8 T Cells between Sustainers and Decayers, Related to Figure 4**

(A) Representative flow plots illustrating the gating strategy used to define the CD8 T cell ( $CD3^+CD4^+CD8^+$ ) populations measured, including naive ( $CD45RA^+CD27^+CCR7^+CD95^-$ ), central memory (CM,  $CD45RA^-CD27^+CCR7^+$ ), effector memory 1 (EM1,  $CD45RA^-CD27^+CCR7^-$ ), effector memory 2 (EM2,  $CD45RA^-CD27^-CCR7^+$ ), effector memory 3 (EM3,  $CD45RA^-CD27^-CCR7^-$ ), and CD45RA<sup>+</sup> effector memory (EMRA,  $CD45RA^+CD27^-CCR7^-$ ).

(B–F) Quantification of the CD8 T cell populations among PBMCs from sustainers ( $n = 11$ ) and decayers ( $n = 10$ ) in draw 1 (E) and draw 3 (F). Means are represented as horizontal lines in the plots. No significant differences were found by Mann-Whitney U test.

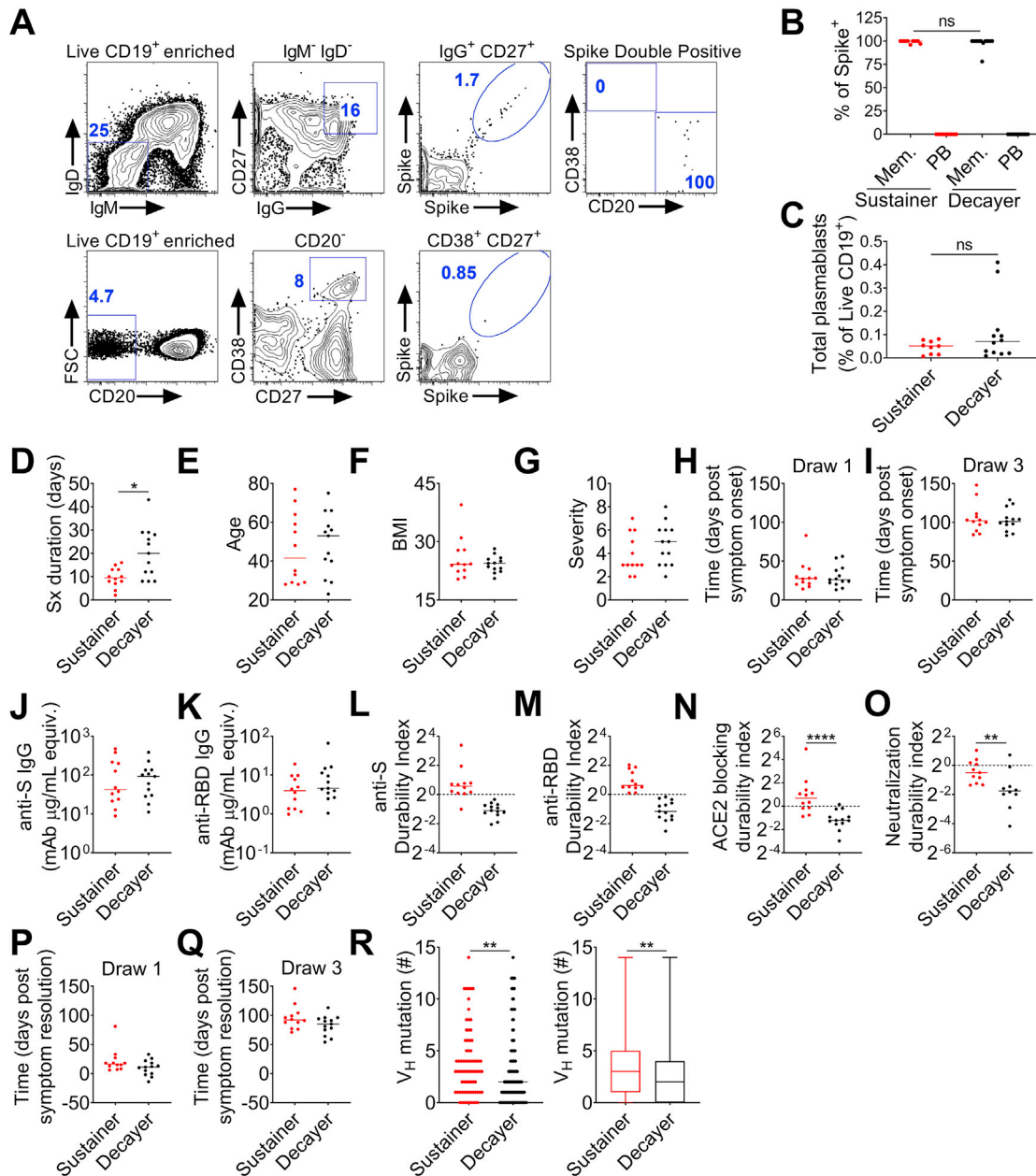


**Figure S7. Confirmation that S-Binding CD19<sup>+</sup>IgM<sup>-</sup>IgD<sup>-</sup>CD27<sup>+</sup>IgG<sup>+</sup>Spike<sup>+</sup> Cells Are Not Plasmablasts and Comparison of Clinical and Antibody Features of Sustainers and Decayers Included in Antibody Sequence Analysis, Related to Figure 5**

(A–C) PBMCs from the first blood draw from sustainers (red,  $n = 9$ ) and decayers (black,  $n = 12$ ) were analyzed by flow cytometry to ascertain whether spike-binding CD19<sup>+</sup> cells (IgM<sup>-</sup>IgD<sup>-</sup>CD27<sup>+</sup>IgG<sup>+</sup>Spike<sup>+</sup>) are memory cells or plasmablasts in subjects analyzed for SHM. (A) Flow plots illustrating the gating strategy to determine the spike-binding CD19<sup>+</sup> cell type are shown on top, with sequential gating shown left to right. IgM<sup>-</sup>IgD<sup>-</sup>CD27<sup>+</sup>IgG<sup>+</sup>Spike<sup>+</sup> cells were analyzed for CD20 and CD38 expression to identify memory cells (CD20<sup>+</sup>CD38<sup>int/low</sup>) and plasmablasts (CD20<sup>-</sup>CD38<sup>hi</sup>). Bottom plots show a second gating approach to confirm that plasmablasts (CD20<sup>-</sup>CD27<sup>+</sup>CD38<sup>hi</sup>) could be identified among PBMCs from the same subjects using this antibody panel. (B) Quantitation of the proportion of IgM<sup>-</sup>IgD<sup>-</sup>CD27<sup>+</sup>IgG<sup>+</sup>Spike<sup>+</sup> memory cells (Mem.) or plasmablasts (PB) among the sustainers and decayers. (C) Quantitation of total plasmablasts as a proportion of all live CD19<sup>+</sup> cells for sustainers and decayers.

(D–Q) Comparison of (D) symptom duration, (E) age, (F) BMI, (G) severity, (H) timing of initial blood draw relative to symptom onset, (I) timing of third blood draw relative to symptom onset, (J) initial anti-S IgG level, (K) initial anti-RBD IgG level, (L) anti-S durability index, (M) anti-RBD durability index, (N) ACE2-inhibition durability index, (O) conventional neutralization durability index, (P) timing of initial blood draw relative to symptom onset, and (Q) timing of third blood draw relative to symptom onset between the sustainers (red,  $n = 12$ ) and decayers (black,  $n = 13$ ) included in the analysis of S-specific memory B cell IgH sequences (Figure 6).

---

(R) Dot plots (left) and box and whisker plots (right) showing mutation numbers per sequence in the VH of sorted S+ single memory B cells with less than 15 V<sub>H</sub> mutations from sustainers (red, n = 12) and decayers (black, n = 13). Significance testing for initial antibody levels used Student's t test on log transformed data. Significance testing for all other comparisons used the Mann-Whitney U test. Significance is reported in the panels, ns not significant, \*p < 0.05, \*\*p < 0.01, \*\*\*p < 0.001, and \*\*\*\*p < 0.0001.